

OBSERVATION SYSTEM FOR PUERTO RICO COASTAL WAVE ANALYSIS

by

Mykola Vysotskyy

A thesis submitted in partial fulfillment of the requirements for the degree of

MASTER OF SCIENCE

in

Computer Engineering

UNIVERSITY OF PUERTO RICO

MAYAGÜEZ CAMPUS

2005

Approved by:

Ramón Vásquez Espinosa, PhD
President, Graduate Committee

Date

Robin G. Williams, PhD
Member, Graduate Committee

Date

Robert Acar, PhD
Member, Graduate Committee

Date

Lev Steinberg, PhD
Representative of Graduate Studies

Date

Isidoro Couvertier, PhD
Chairperson of the Department

Date

ABSTRACT

The National Weather Service in San Juan receives wave model output for the Puerto Rican regional coastal waters generated by WaveWatch III model of National Centers for Environmental Prediction (NCEP). These predictions are often unreliable mainly due to the fact that *in-situ* observations are not available for the coastal regions of Puerto Rico. These observations are required for calibration and validation of the wave model predictions.

This thesis proposes the use of video cameras to collect images of the nearshore zone of the ocean and the development of an algorithm for processing that video data. The algorithm is based on Fast Fourier Transformation, which allows definition of periodic properties of the objects with different gray-scale intensity levels. The output produced by the algorithm includes estimates of wave parameters, such as period and direction in real-world physical units.

RESUMEN

El Servicio Meteorológico Nacional en San Juan recibe la salida de modelo de onda para el aguas costeras regionales Puertorriqueñas generadas por WaveWatch III del modelo de NCEP. Estas predicciones son a menudo no confiables principalmente debido a que *in-situ* observaciones no están disponibles para las regiones costeras de Puerto Rico. Estas observaciones son requeridas para calibración y validación de las predicciones de modelo de onda.

Esta tesis propone usar cámaras de vídeo para coleccionar imágenes de la zona de costera y desarrollar un algoritmo para procesar los datos de vídeo. El algoritmo es diseñado basado en la Transformación Rápida de Fourier, que permite definir propiedades periódicas de los objetos con niveles de intensidad de escala gris diferentes. El algoritmo produce una salida que incluye estimaciones de parámetros de onda, como período y dirección en unidades físicas reales.

To my family and friends

ACKNOWLEDGEMENTS

I want to express my sincere thanks to my advisors Dr. Robin G. Williams and Dr. Ramon Vasquez, and also special thanks to my co-advisors Dr. Robert Acar and Mr. Scott Stripling for their invaluable contributions.

I am also grateful to Rita Peralta of United Technologies in Isabela and to Harry and Lisa Rodriguez of *Tres Sirenas* Hotel in Rincón for allowing me to install video cameras on their properties.

I want to thank my friend Leonid Tolstoy who is responsible for my coming to Puerto Rico and who helped me in times of difficulty. Last, but not least, I would like to thank my family, for their unconditional support, inspiration, and love.

Support for this research has been provided by grants to the University of Puerto Rico at Mayaguez [UPRM] from the National Oceanic and Atmospheric Administration Cooperative Remote Sensing Science and Technology Center [NOAA-CREST] and the National Aeronautics and Space Administration Experimental Program to Stimulate Competitive Research [NASA-EPSCoR]. I wish to thank the administrators of these grants, Mr. Pieter Van der Meer, and Mr. William Martinez.

Table of Contents

ABSTRACT	II
RESUMEN	III
ACKNOWLEDGEMENTS.....	V
TABLE OF CONTENTS.....	VI
TABLE LIST	VIII
FIGURE LIST	IX
1 INTRODUCTION	1
1.1 SCOPE	1
1.2 INTRODUCTION	1
1.3 MOTIVATION.....	2
1.3.1 <i>Climate change and increasing wave height</i>	2
1.3.2 <i>Wave climate around Puerto Rico</i>	3
1.3.3 <i>Operational wave forecasting around Puerto Rico</i>	4
1.3.4 <i>Virtual buoys around Puerto Rico</i>	6
1.3.5 <i>Summary from the above chapters</i>	8
1.4 SUMMARY OF CHAPTERS IN THESIS	8
2 LITERATURE REVIEW	10
3 THEORETICAL BACKGROUND.....	18
3.1 SCOPE	18
3.2 DIGITAL IMAGE PROCESSING	18
3.2.1 <i>What is digital image processing?</i>	18
3.2.2 <i>Image acquisition using sensor array</i>	19
3.2.3 <i>A simple image formation model</i>	19
3.2.4 <i>Image sampling and quantization</i>	20
3.2.5 <i>Representing digital images</i>	20
3.2.6 <i>Processing image in frequency domain</i>	22
3.2.7 <i>Discrete Fast Fourier Transformation</i>	23
3.2.8 <i>Perspective transformation</i>	29
3.2.9 <i>Camera imaging model</i>	32
3.3 WAVE KINEMATICS	34
4 DATA SIMULATION.....	38
4.1 SCOPE.....	38
4.2 SIMULATION OF THE WAVES.....	38
4.2.1 <i>One-wave-train simulation</i>	38
4.2.2 <i>Three-wave-train simulation</i>	41
5 REAL IMAGE ACQUISITION	45

5.1	SCOPE	45
5.2	DESCRIPTION OF AN OBSERVATION SYSTEM	45
5.2.1	<i>Observation system diagram</i>	45
5.2.2	<i>Observation system components</i>	46
5.2.3	<i>Location requirements</i>	49
5.2.4	<i>System mounting</i>	52
6	REAL IMAGE PROCESSING	55
6.1	SCOPE.....	55
6.2	ALGORITHM DESCRIPTION.....	55
6.2.1	<i>Image preprocessing</i>	55
6.2.2	<i>Obtaining wave period and wave direction</i>	57
6.2.3	<i>Obtaining relative wave height</i>	61
7	SYSTEM VALIDATION	64
7.1	SCOPE.....	64
7.2	VALIDATION METHOD DESCRIPTION	64
7.2.1	<i>Introduction</i>	64
7.2.2	<i>Pressure sensor overview</i>	64
7.2.3	<i>Pressure sensor deployment</i>	66
7.2.4	<i>Reading pressure data</i>	66
7.2.5	<i>Pressure data analysis</i>	67
7.2.6	<i>System validation</i>	68
8	CONCLUSIONS AND FUTURE WORK	69
	BIBLIOGRAPHY	70
	APPENDIX	72

Table List

Tables	Page
TABLE 2.1 Normalized wavelet variance.....	16
TABLE 5.1 Equipment list	47

Figure List

Figures	Page
Figure 1.1 Percentage increase in significant wave height.....	2
Figure 1.2 Beach erosion on the West part of the island.....	3
Figure 1.3 Model representation of winds with the geography of Puerto Rico.....	4
Figure 1.4 Raw output with a script run on the raw file.....	5
Figure 1.5 Edited wave model output.....	6
Figure 1.6 Virtual buoys around the island.....	7
Figure 1.7 Report from a virtual buoy.....	7
Figure 2.1 Argus station.....	11
Figure 2.2 "Snap" image.....	12
Figure 2.3 "Timex" image.....	12
Figure 2.4 Sample wave images.....	14
Figure 2.5 Re-oriented wave images based on the results of the wave orientation.....	14
Figure 2.6 ERS-1 SAR image used as test data.....	15
Figure 3.1 Coordinate convention used in this thesis.....	21
Figure 3.2 Original image in spatial domain.....	27
Figure 3.3 Image in frequency domain.....	28
Figure 3.4 Basic imaging system model.....	30
Figure 3.5 Camera imaging model.....	33
Figure 3.6 Phase lines of a two-dimensional wave signal at a given time.....	36
Figure 4.1 Ideal simulated image.....	39
Figure 4.2 Power spectrum of the simulated image in 3-D.....	40
Figure 4.3 Power spectrum of the simulated image in 2-D.....	41
Figure 4.4 Three-wave-train simulated image.....	42
Figure 4.5 Power spectrum of the three-wave-train simulated image in 3-D.....	43
Figure 4.6 Power spectrum of the three-wave-train simulated image in 2-D.....	43
Figure 5.1 Schematic top view of the system.....	46
Figure 5.2 Schematic side view of the system.....	46
Figure 5.3 Connected components of the observation system.....	47
Figure 5.4 Location of the observation system.....	50
Figure 5.5 Aerial view of the site.....	51
Figure 5.6 Isabela bathymetry chart.....	52
Figure 5.7 Front view of the mounted camera.....	53
Figure 5.8 Side view of the camera.....	53
Figure 5.9 Image from the video camera.....	54
Figure 6.1 Image preprocessing stages.....	55
Figure 6.2 Cropped gray-scale image.....	56
Figure 6.3 Orthogonal view image.....	57
Figure 6.4 Image processing final stages.....	58
Figure 6.5 Power spectrum of the image in 3-D.....	58
Figure 6.6 Power spectrum of the image in 2-D.....	59

Figure 6.7 Object location.....	61
Figure 6.8 Time series of intensity power peaks	62
Figure 6.9 Pressure time series	63
Figure 7.1 DST milli pressure sensor	65
Figure 7.2 Pressure sensor attached to a rock	66
Figure 7.3 Power spectrum of the pressure time series	67

List of Symbols and Abbreviations

Abbreviation	Description
CCD	Charged-Coupled Device
DFT	Discrete Fourier Transform
DOS	Disk Operating System
FFT	Fast Fourier Transformation
FTP	File Transfer Protocol
GPS	Global Positioning System
HTTP	Hyper Text Transfer Protocol
ISP	Internet Service Provider
IP	Internet Protocol
NCEP	National Centers for Environmental Prediction
NWS	National Weather Service
PC	Personal Computer
PR	Puerto Rico
VGA	Video Graphics Array
2-D	Two Dimensional
3-D	Three Dimensional

1 INTRODUCTION

1.1 Scope

This chapter contains an overview of the thesis as well as a description of the nature, justification, and objectives of the present research work.

1.2 Introduction

Data acquisition using video-capturing equipment is becoming more and more popular in many fields, especially when it is possible to substitute automated computer vision systems for human involvement in routine work. The present research proposes to use image-processing techniques on data recorded by video cameras to obtain real-time estimates of ocean-wave parameters in the nearshore zone of Puerto Rico [PR]. We believe the proposed research will provide a significant step in the field of oceanography and will help oceanographers, meteorologists, and others related to marine commercial interests or scientific applications.

Practically speaking, the hardware used in this project might replace buoys that are of order ten times more expensive, or radar and satellite equipment that is of order a hundred times more expensive. Some restrictions will apply, but this equipment and these procedures have a clear application for surface analysis in ocean areas. As with any apparatus there will be problems involving maintenance. Furthermore, to obtain a useful image of the nearshore zone with well-defined waves—that is, those that can be classified into objects and noise—the cameras must be optimally located. For example, they must be pointed at areas in the nearshore zone where the waves have not yet been affected by

the reefs. At times it may be difficult to find a secure place in a specific location to install the system. Nevertheless, such problems are normally solvable. In the case of the present research project, for example, on two occasions it was necessary first to establish a friendly relationship with owners before mounting cameras on their property.

1.3 Motivation

1.3.1 Climate change and increasing wave height

Wave heights in the world's oceans (e.g., Atlantic) are clearly rising, most likely due to climate change brought about by global warming.

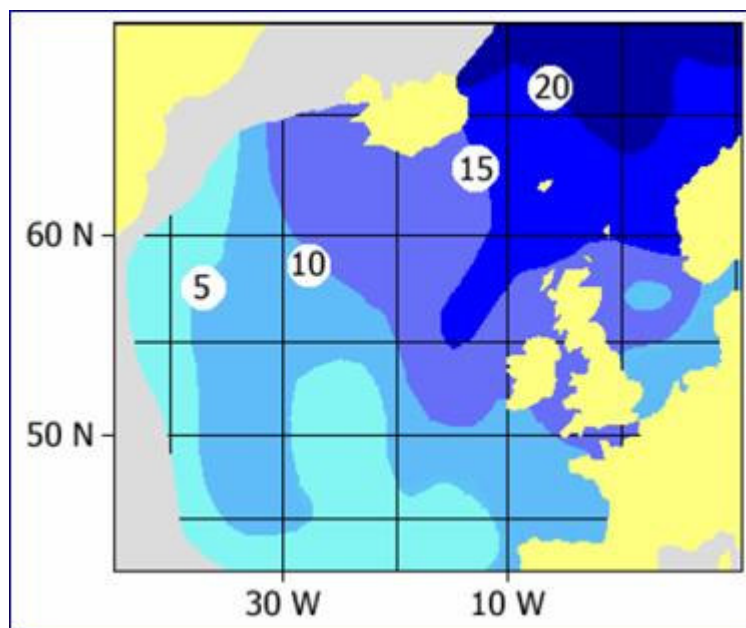


Figure 1.1 Percentage increase in significant wave height

Figure 1.1 shows the percentage increase in significant wave height—the average height of the highest third of the waves—in the North Atlantic during the winter months (December to February) between the periods 1985-1989 and 1991-1996. Note the short periods over which data are averaged [1].

1.3.2 Wave climate around Puerto Rico

In Puerto Rico there is evidence in recent years that both wave activity and wave height are also changing.

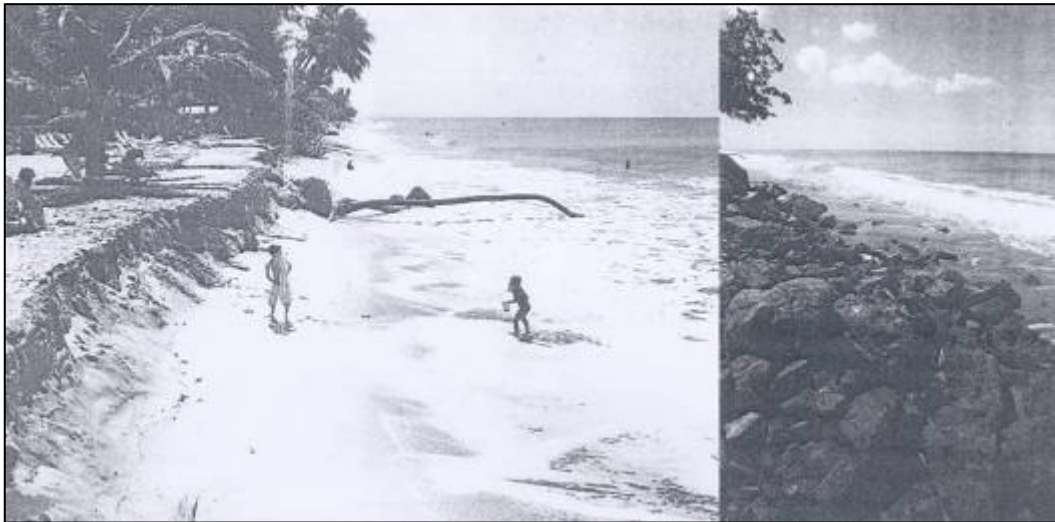


Figure 1.2 Beach erosion on the West part of the island

Observations from the surfing community in Puerto Rico suggest that wave heights in the 60s, 70s, and 80s during the winters were larger and wave occurrences more frequent than they have been during the last ten years.

Storms in 1988, Hurricane Hugo (1989), and the Halloween storm of 1991 have all had a significant impact on the North and Northwestern coastlines, altering the beaches and the nearshore bathymetry [2].

1.3.3 Operational wave forecasting around Puerto Rico

Every six hours NCEP's WaveWatch III model provides the San Juan NWS with predictions of wave conditions for the Puerto Rican coastline. Figure 1.3 displays wind patterns associated with the geography of PR and the Virgin Islands, as seen by the model. The resolution is 0.25 deg X 0.25 deg.

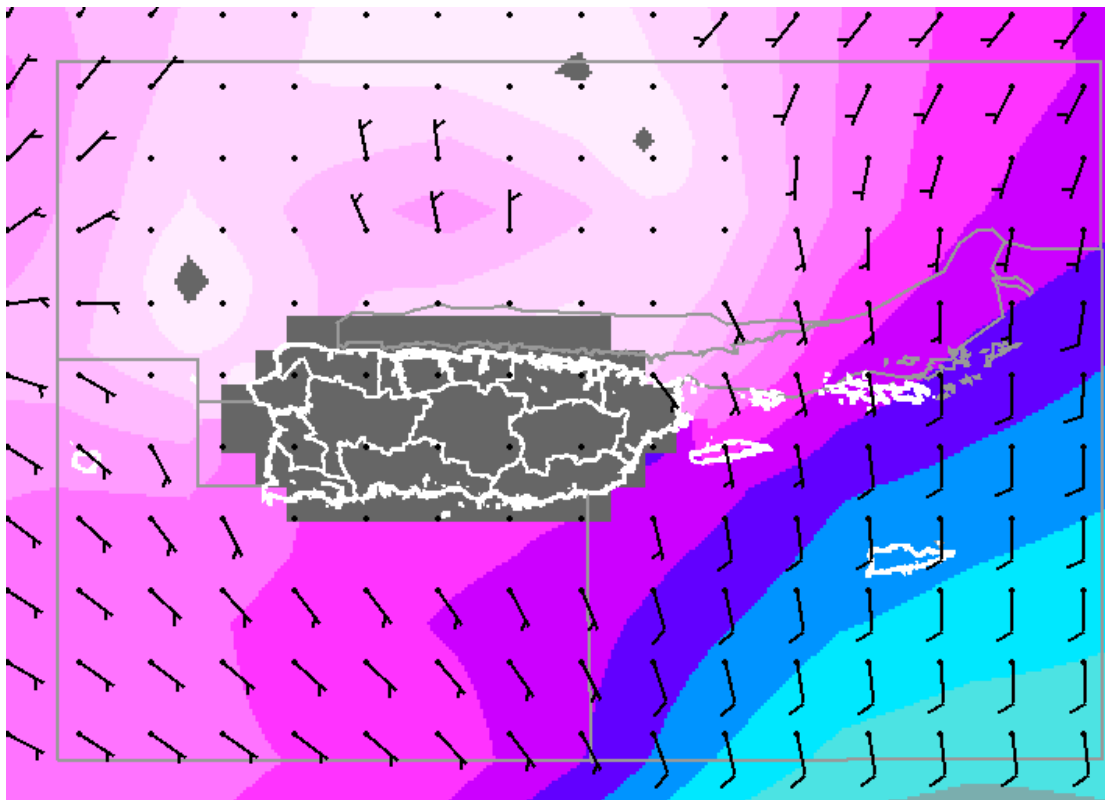


Figure 1.3 Model representation of winds with the geography of Puerto Rico

Figure 1.4 does not represent the original raw output but shows the result of a script run on the raw file to fill in the wave heights off the coast using real geography. Unfortunately, the model resolution is not high enough to resolve the bathymetry of PR and the Caribbean accurately. Consequently, significant editing of the WaveWatch III model output is necessary to produce an accurate and realistic depiction of wave parameters in the region.

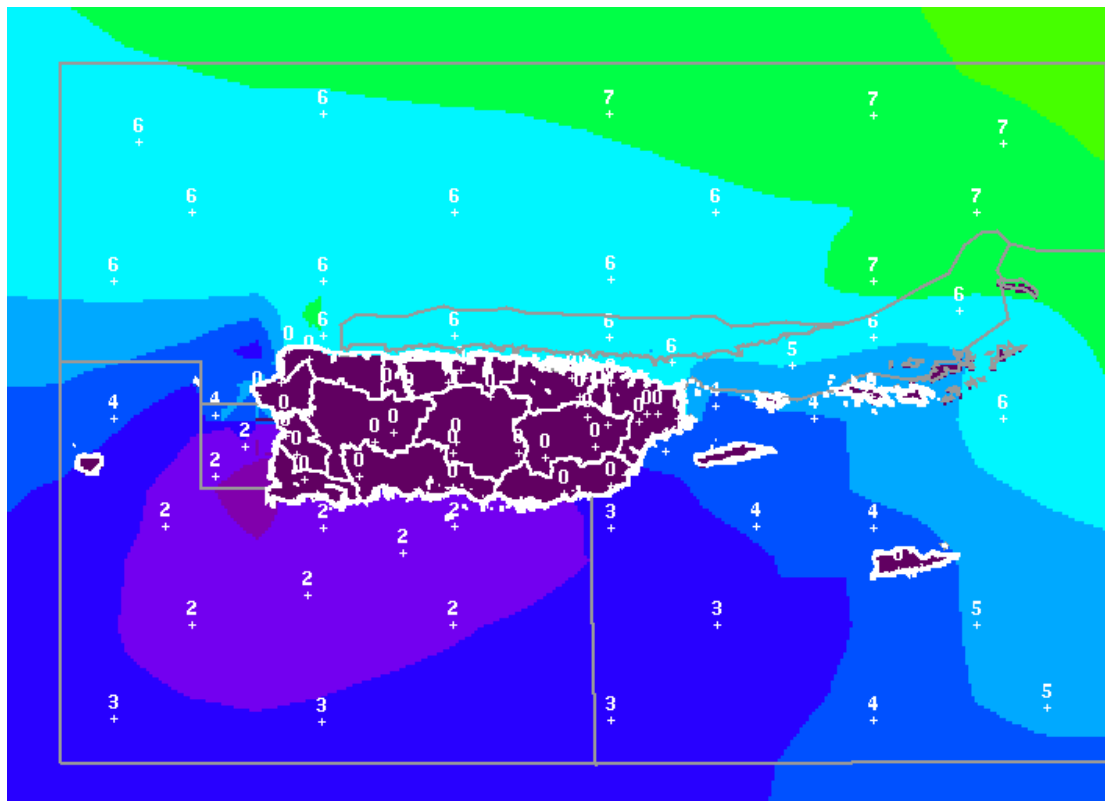


Figure 1.4 Raw output with a script run on the raw file

Figure 1.5 is a chart of wave model output based on meteorologist Scott Stripling's eleven years of experience in marine forecasting around PR.

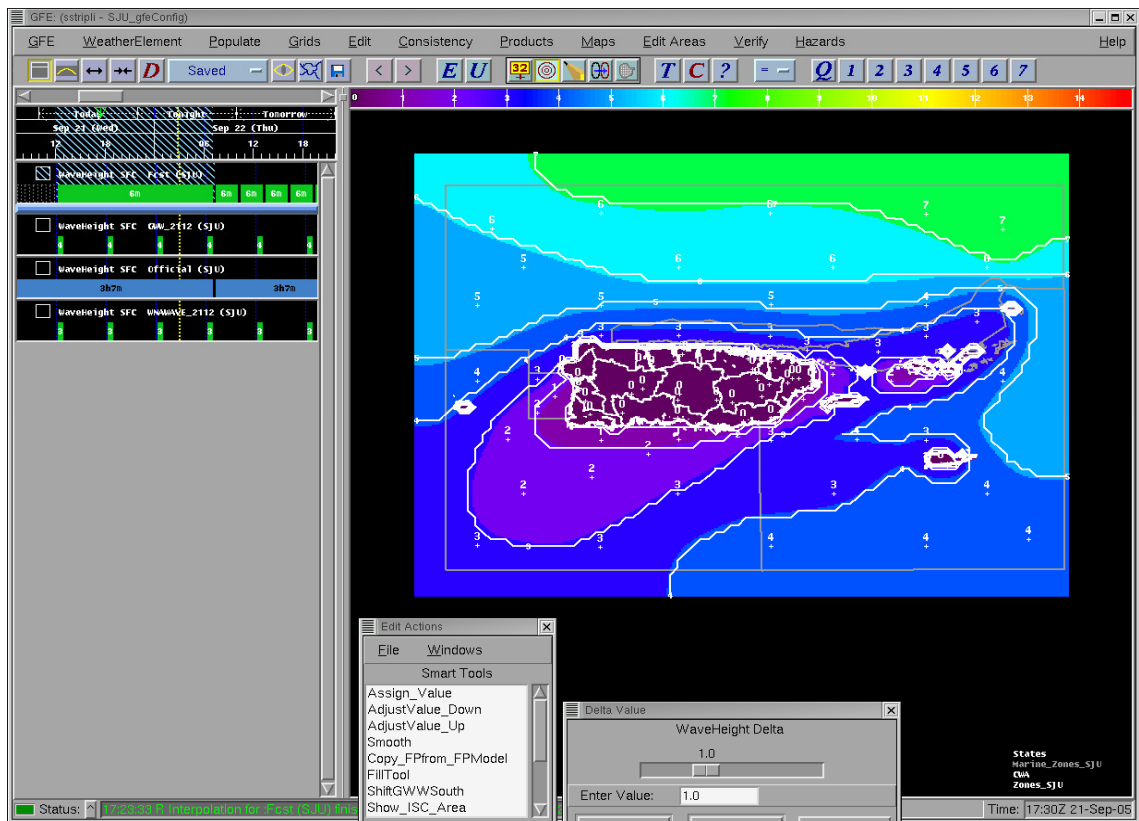


Figure 1.5 Edited wave model output

1.3.4 Virtual buoys around Puerto Rico

Since no operating buoys are actively deployed in the nearshore waters around the island of Puerto Rico, anyone interested in local marine forecasts must obtain them from the so called “virtual buoys” via the Internet at <http://buoyweather.com/>.



Figure 1.6 Virtual buoys around the island

Virtual buoy reports display wave height, wave direction, periodicity, wind speed, and wind direction that have been extracted from the WaveWatch III model (Figure 1.7).

The data is not reliable because it is taken from the raw model output.

DAY HOUR	28 1pm	28 7pm	29 1am	29 7am	29 1pm	29 7pm	30 1am	30 7am	30 1pm	30 7pm	31 1am	31 7am	31 1pm	31 7pm	1 1am	1 7am
OPEN OCEAN SEAS & SWELL (ft)																
peak Hs	2	2	2	2	2	2	2	2	2	2	2	2	3	3	3	3
PERIOD	4	9	4	8	7	6	6	9	8	8	8	7	5	5	5	5
PRIMARY DIRECTION	ESE	ENE	E	ENE	NNE	NNE	NNE	ENE	NE	NE	NE	NE	SE	SE	SSE	SE
WIND RANGE (knots)																
gust	8	10	7	6	7	6	6	7	10	8	9	10	12	15	14	15
sust.	6	7	5	5	5	5	4	5	8	6	6	7	9	11	10	11
WIND DIRECTION	E	E	ESE	ENE	E	ESE	ESE	ESE	SSE	ESE	ESE	ESE	SE	E	ESE	ESE

Figure 1.7 Report from a virtual buoy

1.3.5 Summary from the above chapters

Two main issues arise in the study of wave climate around Puerto Rico:

- Detection of Climate Change. Long-term wave measurements are needed for future use in Caribbean climate studies.
- WaveWatch III Model Validation and Calibration. Wave model prediction needs to be validated by *in-situ* observations which are presently not available for the coastal regions of Puerto Rico.

To address both issues, the development of a video-observation system and algorithms for processing such video data is proposed. The data will be recorded in daylight by video camera and processed by algorithms in real time. These algorithms will estimate wave parameters such as periodicity, direction, and height.

1.4 Summary of Chapters in Thesis

A description of the nature, justification, and objectives of the present research work are presented in Chapter 1.

Chapter 2 presents a review of the publications and literature relevant to the research.

Chapter 3 describes the theoretical background related to this research. This discussion includes: definition of a digital image, the basics of image processing in

frequency domain (Fast Fourier Transformation), perspective on orthogonal transformation equations, and the basics of wave kinematics.

Chapter 4 describes the simulation of the data including both one-wave-train and three-wave-train simulations and how they are processed in a wavenumber domain.

Chapter 5 presents the stages involved in retrieving the nearshore sea surface wave image from a video camera and the transferring of it to a server. It includes a description of an observation system, both its installation and testing.

Chapter 6 describes in detail the algorithm used to obtain wave parameters, such as a wavelength and a wave direction.

Chapter 7 delineates the method based on recording pressure data used to validate the system.

Chapter 8 presents the conclusions of the present research and suggestions for future work.

The Appendix contains listings for the programs, written in MatLab, used in this research; it also gives specifications for the equipment used in this research.

2 LITERATURE REVIEW

A number of previous pertinent studies of ocean surface wave analysis based on video and radar data exist. The review in this chapter will focus on the most significant of these.

Over the past two decades, Rob Holman and his team of scientists from the Coastal Imaging Lab at Oregon State University have evolved video data processing techniques into Argus, a program which currently samples twelve of the approximately thirty global sites operating in eight countries. Starting in 1992, first-generation Argus Stations had cameras connected to a PC running DOS but this system did not address their needs well. Although the second generation system moved to a substantially more powerful Silicon Graphics Unix workstation in 1997, most of the computation and intelligence still resided in the lab and was implemented through post-processing. Internet sensors, and their potential advantages, were not available at that time. As the Coastal Imaging Lab team shifts to third generation digital cameras and communication, they plan to move intelligence and analysis components out to the sensors. Presently, an Argus Station includes a suite of cameras connected to a host computer which is, in turn, linked to the world by modem and the Internet (Figure 2.1). Argus uses analog cameras connected through a computer-controlled switch [3]. It returns images of two types.

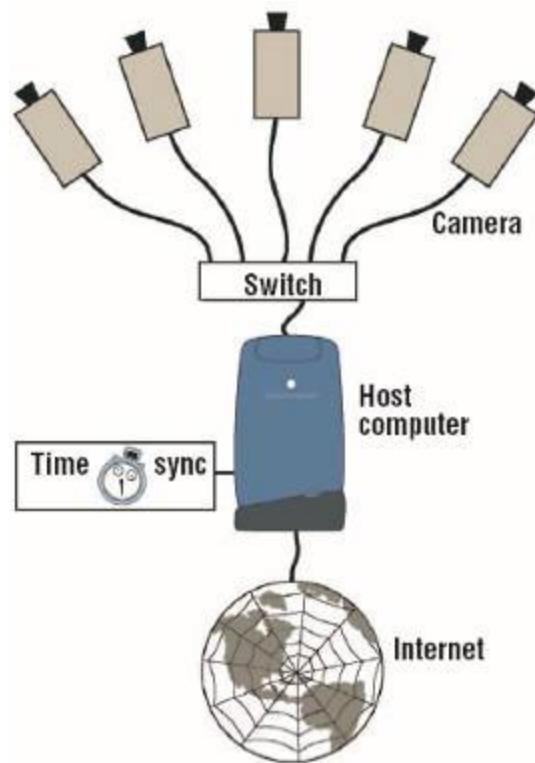


Figure 2.1 Argus station

The first type, called "snaps," are snapshot images of the beach or cliff. These images are oblique camera shots taken from a specific nearshore region, typically at hourly intervals during daylight hours (Figure 2.2).



Figure 2.2 "Snap" image

A "timex" image is a single image constituted from an average of images gathered over a ten-minute period of time. Such time-exposure images have proved useful for detecting a number of nearshore morphological features, including sandbars, rip channels, and changes in shoreline. This averaged view presents a generalized picture of patterns of wave activity in the image by removing the influence of high-frequency wave activity (Figure 2.3) [4].



Figure 2.3 "Timex" image

Several studies of wave direction have involved video cameras. The most recent study was conducted by scientists from the Naval Surface Warfare Center, Panama City, Florida. This research focuses on the visual analysis of waves obtained at a local level, typically a mast mounted camera aboard a ship. While this work deals with the determination of sea-wave orientation, the ultimate goal is to develop a system capable of determining sea-state parameters in near-real time through visual means. Such a system would provide the first step in developing an adaptive mission planner for an unmanned autonomous surface vessel [5].

A wavelet-based algorithm was developed to determine the orientation of the sea waves present in a visual image. Due to the multi-scale nature of the wavelet transform, results are generated for each level in the transform. The wave orientation algorithm uses as its basis the feature preservation property of the 2-D wavelet transform. Given this, a method was developed to select the best sub-band or combination of sub-bands from which to calculate a result. This method employs a weighted average voting system in which contributions from the various sub-bands form to yield a single result.

In Figure 2.4, the left hand image was captured with regular optics while the image on the right was taken with an infrared camera. Images in Figure 2.5 show the result of re-orienting the images from Figure 2.4 using the results from the wave orientation and best basis algorithms. As can be seen, the features present in each image line up with the horizontal axis verifying the results.

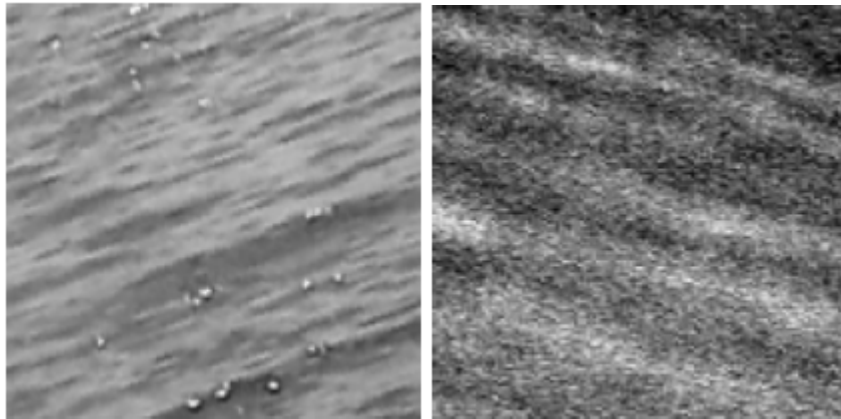


Figure 2.4 Sample wave images

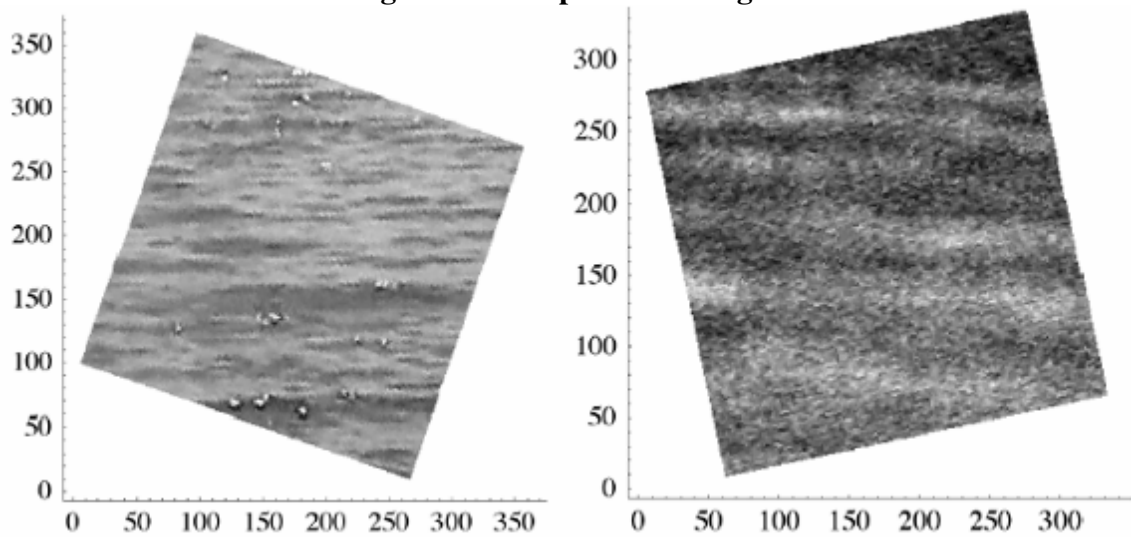


Figure 2.5 Re-oriented wave images based on the results of the wave orientation

Generally speaking, the idea of this research is to re-orient the image using a wavelet based method.

Another study of interest to the present research is based on the retrieval of wave parameters using synthetic aperture radar [SAR] images of ocean waves. Unlike most of the Earth's surface features, ocean waves are moving targets which cause the generation

of special signatures in the image at the time it is formed by the SAR processor [6]. This form of research approaches the retrieval of wave parameters by determining the wave spectrum from SAR images using wavelet analysis. Unlike *sines* and *cosines* used in Fourier analysis, the wavelet basis for these functions is localized in both time and frequency, allowing for the analysis of nonperiodic series where data experience abrupt variations or high frequencies, and signals of different scales are hidden in a much longer sequence.

The data source was a segment of an ERS-1 SAR image corresponding to the Pacific coast of Baja California, Mexico. The image in Figure 2.6, oriented toward North at the top, displays a well developed swell traveling from West to East.



Figure 2.6 ERS-1 SAR image used as test data

Table 2.1 shows the normalized wavelet variance for each detail level and its associated physical scale. R^{Tilt} and R^{hydro} are the main imaging mechanisms for waves traveling in range, hence the authors of this paper suppose that they are the principal contributors to the series. From Table 2.1 we can see that details 2, 3, and 4 hold the maximum power in the series and probably are related to R^{Tilt} , since reflectivity increases as the wave reaches the coast due to change in wave slope. On the other hand, details 5 and 6 yield a smaller power to the total variance and, as they tend to diminish toward the coast, are probably related to R^{hydro} . It can also be seen that the dominant wavelength is 100 meters, followed by 50 and 200 wavelengths which are typical in coastal regions.

TABLE 2.1 Normalized wavelet variance

Detail Level	Physical Scale (m)	Norm. Variance
7	1600	0.04012
6	800	0.04001
5	400	0.07755
4	200	0.16580
3	100	0.32902
2	50	0.26444
1	25	0.08306

Although there exist more studies and research involving the estimation of wave parameters based on data from optical and radar remote sensing devices, such as video

cameras and radar, the ones reviewed above are the most significant for the present research. The methods and approaches offered in other studies are based on different techniques and different types of acquisition equipment.

3 THEORETICAL BACKGROUND

3.1 Scope

This chapter presents a detailed description of the image processing algorithm based on the Discrete Fast Fourier Transformation, the perspective transformation used in this research; it also provides readers with some basic information about wave kinematics in the field of oceanography.

3.2 Digital Image Processing

3.2.1 *What is digital image processing?*

We can describe an image as a two-dimensional function, $f(x, y)$, where x and y are spatial (plane) coordinates, and the amplitude of f at any pair of coordinates (x, y) is called the intensity or gray level of the image at that point. When x , y , and the amplitude values of f are all finite, discrete quantities, we call the image a digital image. The field of digital image processing refers to processing digital images by means of a digital computer. Note that a digital image is composed of a finite number of elements, each of which has a particular location and value. These elements are referred to as “picture elements,” “image elements,” “pels,” and “pixels.” “Pixel” is the term most widely used to denote the elements of a digital image [7].

3.2.2 Image acquisition using sensor array

Sensing devices are frequently arranged in an array format. This format is also the predominant arrangement found in digital cameras. A typical sensor for these cameras is a CCD array, which can be manufactured with a broad range of sensing properties and can be packaged in rugged arrays of elements or more. CCD sensors are used widely in digital cameras and other light sensing instruments. The response of each sensor is proportional to the integral of the light energy projected onto the surface of the sensor, a property that is used in astronomical applications and others that require low noise images. Noise reduction is achieved by letting the sensor integrate the input light signal over minutes or even hours [7].

The first function performed by an imaging system is to collect the incoming energy and focus it onto an image plane. If the energy is in the form of light, the front end of the imaging system is a lens, which projects the viewed scene onto the focal plane of the lens. The output of the sensor array, which is coincident with the focal plane, is proportional to the integral of the light received at each sensor. Digital and analog circuitry sweep these outputs and convert them to a video signal, which is then digitized by another section of the imaging system [7].

3.2.3 A simple image formation model

As previously described, images may be denoted by the two-dimensional functions of the form $f(x, y)$. The value or amplitude of f at spatial coordinates (x, y) is a positive

scalar quantity whose physical meaning is determined by the source of the image. Most of the images of interest to this research are monochromatic images, whose values are said to span the gray scale. When an image is generated from a physical process, its values are proportional to the energy radiated by a physical source (e.g., electromagnetic waves). As a consequence, $f(x, y)$ must be nonzero and finite; that is,

$$0 < f(x, y) < q \quad \mathbf{3.1}$$

The function $f(x, y)$ may be characterized by two components: (1) the amount of source illumination incident to the scene being viewed, and (2) the amount of illumination reflected by the objects in the scene. Appropriately, these are called the illumination and reflectance components and are denoted by $i(x, y)$ and $r(x, y)$, respectively [7].

3.2.4 Image sampling and quantization

The output of most sensors is a continuous voltage waveform whose amplitude and spatial behavior are related to the physical phenomenon being sensed. To create a digital image we need to convert the continuous sensed data into digital form. This involves two processes: sampling and quantization. In digital cameras, these two processes are implemented in the hardware [7].

3.2.5 Representing digital images

The result of sampling and quantization is a matrix of real numbers. Two principal methods will be used here to represent digital images. Assume that an image $f(x, y)$ is

sampled so that the resulting digital image has M -rows and N -columns. The values of the coordinates (x, y) now become discrete quantities. For notational clarity and convenience, we shall use integer values for these discrete coordinates. Thus, the values of the coordinates at the origin are $(x, y) = (0, 0)$. The next coordinate values along the first row of the image are represented as $(x, y) = (0, 1)$. It is important to keep in mind that the notation $(0, 1)$ is used to signify the second sample along the first row and not that these are the actual values of the physical coordinates when the image was sampled.

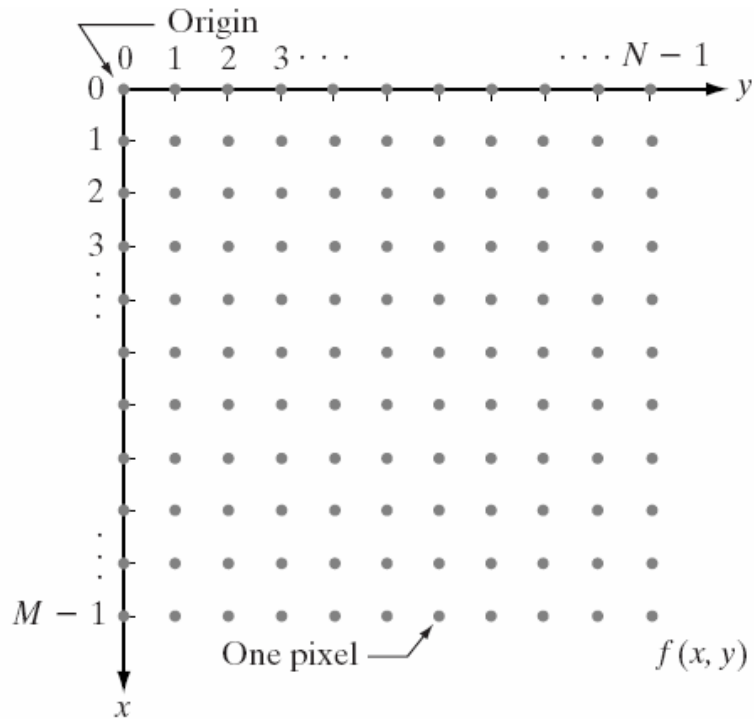


Figure 3.1 Coordinate convention used in this thesis

The notation introduced in the preceding paragraph allows us to write the complete $M*N$ digital image in the following compact matrix form (Eq. 3.2):

$$f(x, y) = \begin{bmatrix} f(0,0) & f(0,1) & \dots & f(0,N-1) \\ f(1,0) & f(1,1) & \dots & f(1,N-1) \\ \vdots & \vdots & \vdots & \vdots \\ f(M-1,0) & f(M-1,1) & \dots & f(M-1,N-1) \end{bmatrix} \quad \mathbf{3.2}$$

By definition, the right side of this equation is a digital image. Each element of this matrix array are referred to variously as: “image element,” “picture element,” “pixel,” or “pel.” In this thesis the terms “image” and “pixel” will be used throughout the rest of our discussions to denote a digital image and its elements [7].

3.2.6 Processing image in frequency domain

Image processing approaches fall into two broad categories: spatial domain methods and frequency domain methods. The term spatial domain refers to the image plane itself, and approaches in this category are based on direct manipulation of pixels in an image. Frequency domain processing techniques are based on modifying the *Fourier Transform* of an image. Since we process images in frequency domain in this work, we are going to cover some basics of Fourier Transformation of digital images in the next paragraph.

For simplicity, assume that the image I being considered is formed by projection from scene S (which might be a two- or three-dimensional scene, etc.). The frequency domain is a space in which each image value at image position F represents the amount that the intensity values in image I vary over a specific distance related to F . In the frequency domain, changes in image position correspond to changes in the spatial frequency, (or the rate at which image intensity values) are changing in the spatial

domain image I . For example, suppose that there is the value 20 at the point that represents the frequency 0.1 (or 1 period every 10 pixels). This means that in the corresponding spatial domain image I the intensity values vary from dark to light and back to dark over a distance of 10 pixels, and that the contrast between the lightest and darkest is 40 gray levels (2 times 20) [8].

The frequency domain is especially interesting in such cases because:

- it may make explicit periodic relationships in the spatial domain, and
- some image processing operators are more efficient, or indeed offer the only practical solution, when applied in the frequency domain.

3.2.7 Discrete Fast Fourier Transformation

The Fourier Transform is an important image processing tool which is used to decompose an image into its sine and cosine components. The output of the transformation represents the image in the Fourier or frequency domain, while the input image is the spatial domain equivalent. In the Fourier domain image, each point represents a particular frequency contained in the spatial domain image.

The Fourier Transform is used in a wide range of applications, such as image analysis, image filtering, image reconstruction and image compression.

As we are only concerned with digital images, we will restrict this discussion to the Discrete Fourier Transform [DFT].

The DFT is the sampled Fourier Transform and therefore does not contain all frequencies forming an image, but only a set of samples which is large enough to fully describe the spatial domain image. The number of frequencies corresponds to the number of pixels in the spatial domain image, i.e. the image in the spatial and Fourier domain are of the same size [8].

For a square image of size $N \times N$, the two-dimensional DFT is given by:

$$F(k, l) = \frac{1}{N^2} \sum_{i=0}^{N-1} \sum_{j=0}^{N-1} f(i, j) e^{-i2\pi \frac{(ki+lj)}{N}} \quad 3.3$$

where $f(i, j)$ is the image in the spatial domain and the exponential term is the basis function corresponding to each point $F(k, l)$ in the Fourier space. The equation can be interpreted as: the value of each point $F(k, l)$ is obtained by multiplying the spatial image with the corresponding base function and summing the result.

The basis functions are sine and cosine waves with increasing frequencies, i.e. $F(0, 0)$ represents the image mean of the image which corresponds to the average brightness and $F(N-1, N-1)$ represents the highest frequency.

In a similar way, the Fourier image can be re-transformed to the spatial domain. The inverse Fourier transform is given by:

$$f(i, j) = \frac{1}{N^2} \sum_{k=0}^{N-1} \sum_{l=0}^{N-1} F(k, l) e^{i2\pi \frac{(ki+lj)}{N}} \quad 3.4$$

To obtain the result for the above equations, a double sum has to be calculated for each image point. However, because the Fourier Transform is separable, it can be written as:

$$F(k, l) = \frac{1}{N^2} \sum_{j=0}^{N-1} P(k, j) e^{-i2\pi \frac{lj}{N}} \quad 3.5$$

where

$$P(k, j) = \frac{1}{N^2} \sum_{i=0}^{N-1} f(i, j) e^{-i2\pi \frac{ki}{N}} \quad 3.6$$

Using these two formulas, the spatial domain image is first transformed into an intermediate image using N one-dimensional Fourier Transforms. This intermediate image is then transformed into the final image, again using N one-dimensional Fourier Transforms. Expressing the two-dimensional Fourier Transform in terms of a series of $2N$ one-dimensional transforms decreases the number of required computations [8].

Even with these computational savings, the ordinary one-dimensional DFT has N^2 complexity. This can be reduced to $N \log_2 N$ if we employ the Fast Fourier Transform (FFT) to compute the one-dimensional DFTs. This is a significant improvement, in particular for large images. There are various forms of the FFT and most of them restrict the size of the input image that may be transformed, often to $N = 2^n$ where n is an integer. The mathematical details are well described in the literature.

The Fourier Transform produces a complex number valued output image which can be displayed with two images, either with the real and imaginary part or with magnitude and phase. In image processing often only the magnitude of the Fourier Transform is displayed, as it contains most of the information of the geometric structure of the spatial domain image. However, if we want to re-transform the Fourier image into the correct spatial domain after some processing in the frequency domain, we must make sure to preserve both magnitude and phase of the Fourier image [8].

The Fourier domain image has a much greater range than the image in the spatial domain. Hence, to be sufficiently accurate, its values are usually calculated and stored in float values.

We will now experiment with some simple images to better understand the nature of the transform. The response of the Fourier Transform to periodic patterns in the spatial domain images can be seen very easily in the following artificial images.

The image in Figure 3.2 shows 2 pixel wide vertical stripes.

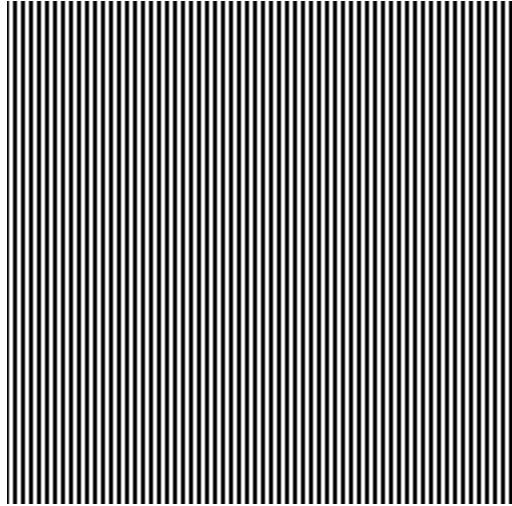


Figure 3.2 Original image in spatial domain

The Fourier transform of the image from Figure 3.2 is shown in Figure 3.3. If we look carefully, we can see that it contains 3 main values: the image mean and, since the Fourier image is symmetrical to its center, two points corresponding to the frequency of the stripes in the original image. Note that the two points lie on a horizontal line through the image center, because the image intensity in the spatial domain changes the most if we go along it horizontally [8].

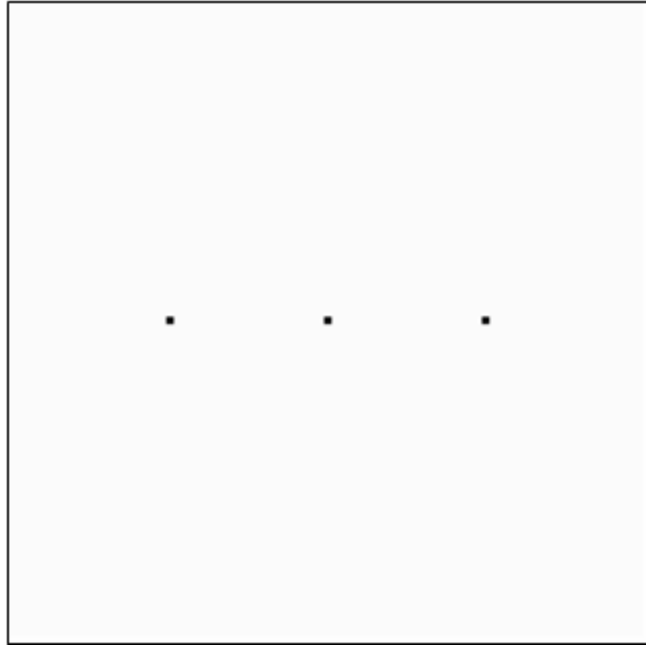


Figure 3.3 Image in frequency domain

The distance of the points to the center can be explained as follows: the maximum frequency which can be represented in the spatial domain are one pixel wide stripes (Eq 3.7).

$$f_{\max} = \frac{1}{1\text{pixel}} \quad 3.7$$

Hence, the two pixel wide stripes in the above image represent

$$f = \frac{1}{2\text{pixel}} = \frac{f_{\max}}{2} \quad 3.8$$

Thus, the points in the Fourier image are halfway between the center and the edge of the image, i.e. the represented frequency is half of the maximum [8].

Further investigation of the Fourier image shows that the magnitude of other frequencies in the image is less than 1/100 of the image mean, i.e. they don't make any significant contribution to the image. The magnitudes of the two minor points are each two-thirds of the image mean [8].

3.2.8 Perspective transformation

Most two-dimensional images are views of three-dimensional scenes from the physical perspective of a camera imaging the scene. It is often desirable to modify an observed image so as to simulate an alternative viewpoint. This can be accomplished by use of a perspective transformation.

Figure 3.4 shows a simple model of an imaging system that projects points of light in three-dimensional object space to points of light in a two-dimensional image plane through a lens focused for distant objects [9].

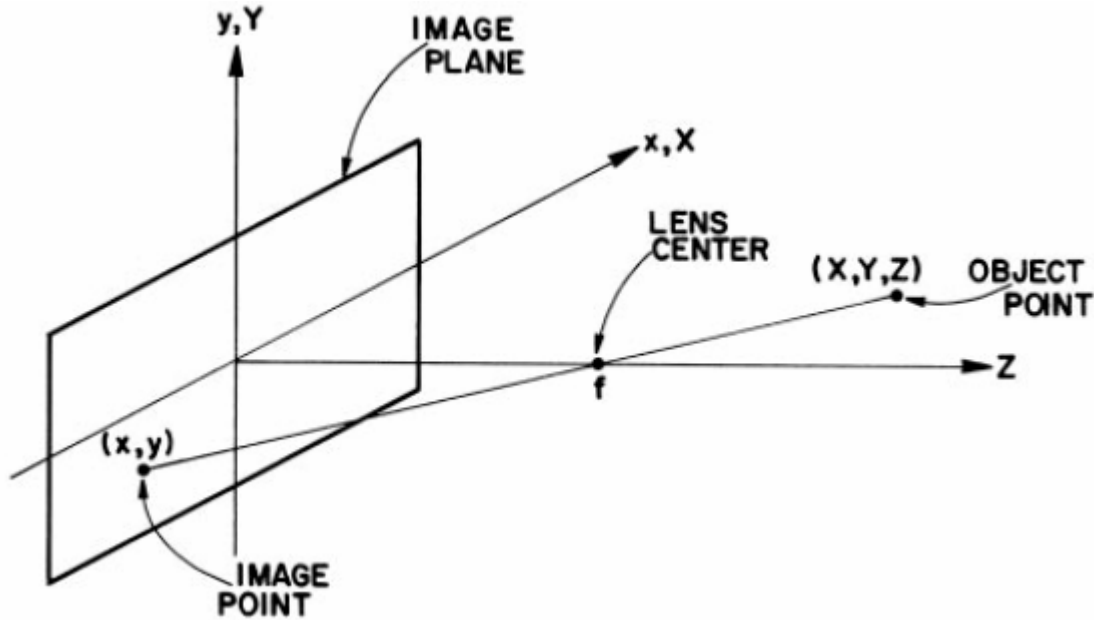


Figure 3.4 Basic imaging system model

Let (X, Y, Z) be the continuous domain coordinate of an object point in the scene, and let (x, y) be the continuous domain-projected coordinate in the image plane. The image plane is assumed to be at the center of the coordinate system. The lens is located at a distance f to the right of the image plane, where f is the focal length of the lens. By use of similar triangles, it is easy to establish that

$$x = \frac{fX}{f - Z} \tag{3.9}$$

$$y = \frac{fY}{f - Z} \tag{3.10}$$

Thus the projected point (x, y) is related nonlinearly to the object point (X, Y, Z) . This relationship can be simplified by utilization of homogeneous coordinates [9].

Let

$$v = \begin{bmatrix} X \\ Y \\ Z \end{bmatrix} \quad \mathbf{3.11}$$

be a vector containing the object point coordinates. The homogeneous vector \tilde{v} corresponding to v is

$$\tilde{v} = \begin{bmatrix} sX \\ sY \\ sZ \\ s \end{bmatrix} \quad \mathbf{3.12}$$

where s is a scaling constant. The Cartesian vector v can be generated from the homogeneous vector \tilde{v} by dividing each of the first three components by the fourth. The utility of this representation will soon become evident [9].

Consider the following perspective transformation matrix:

$$P = \begin{bmatrix} 1 & 0 & 0 & 0 \\ 0 & 1 & 0 & 0 \\ 0 & 0 & 1 & 0 \\ 0 & -1/f & 0 & 1 \end{bmatrix} \quad \mathbf{3.13}$$

Thus, the transformed vector \tilde{w} will be

$$\tilde{w} = P\tilde{v} \quad \mathbf{3.14}$$

It is possible to project a specific image point back into three-dimensional object space through an inverse perspective transformation

$$\tilde{v} = P^{-1}\tilde{w} \quad \mathbf{3.15}$$

3.2.9 Camera imaging model

Figure 3.5 shows an electronic camera in world coordinate space. This camera is physically supported by a gimbal that permits panning about an angle θ (horizontal movement in this geometry) and tilting about an angle ϕ (vertical movement). The gimbal center is at the coordinate (X_G, Y_G, Z_G) in the world coordinate system. The gimbal center and image plane center are offset by a vector with coordinates $(X_\theta, Y_\theta, Z_\theta)$.

If the camera were to be located at the center of the world coordinate origin, not panned nor tilted with respect to the reference axes, and if the camera image plane was not offset with respect to the gimbal, the homogeneous image model would be as derived in the previous paragraph (Eq. 3.14). The camera imaging model can easily be derived by modifying Eq. 3.10 sequentially using a three-dimensional extension of translation and rotation concepts [9].

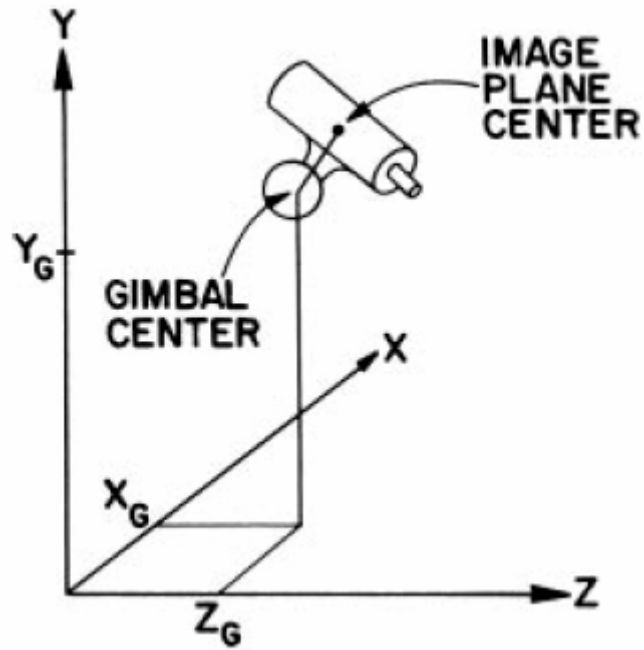


Figure 3.5 Camera imaging model

The offset of the camera to location (X_G, Y_G, Z_G) can be accommodated by the translation operation

$$\tilde{w} = PT_G \tilde{v} \quad 3.16$$

where

$$T_G = \begin{bmatrix} 1 & 0 & 0 & -X_G \\ 0 & 1 & 0 & -Y_G \\ 0 & 0 & 1 & -Z_G \\ 0 & 0 & 0 & 1 \end{bmatrix} \quad 3.17$$

Pan and tilt are modeled by a rotation transformation

$$\tilde{w} = PRT_G \tilde{v} \quad 3.18$$

where

$$R = \begin{bmatrix} \cos \theta & -\sin \theta & 0 & 0 \\ \cos \phi \sin \theta & \cos \phi \cos \theta & -\sin \phi & 0 \\ \sin \phi \sin \theta & \sin \phi \cos \theta & \cos \phi & 0 \\ 0 & 0 & 0 & 1 \end{bmatrix} \quad \mathbf{3.19}$$

Finally, the camera-to-gimbal offset is modeled as

$$\tilde{w} = PT_c RT_G \tilde{v} \quad \mathbf{3.20}$$

where

$$T_G = \begin{bmatrix} 1 & 0 & 0 & -X_o \\ 0 & 1 & 0 & -Y_o \\ 0 & 0 & 1 & -Z_o \\ 0 & 0 & 0 & 1 \end{bmatrix} \quad \mathbf{3.21}$$

Equation 3.20 is the final result giving the complete camera imaging model transformation between an object and an image point. The explicit relationship between an object point (X, Y, Z) and its image plane projection (x, y) can be obtained by performing the matrix multiplications analytically and then forming the Cartesian coordinates by dividing the first two components of \tilde{w} by the fourth [9].

3.3 Wave Kinematics

For simplicity of presentation and easier graphical representation, we will consider here a two-dimensional wave, namely, a physical signal occupying the (x, y) plane and evolving with time t . The prototypical wave form is the sinusoidal function, and so we assume that a physical variable of the system, denoted be a and being pressure, a velocity component or whatever, evolves according to

$$a = A \cos(lx + my - \omega t + \phi) \quad 3.22$$

The coefficient A is the wave amplitude ($-A \leq a \leq +A$), whereas the argument

$$a = lx + my - \omega t + \phi \quad 3.23$$

is called the phase. The latter consists of terms that vary with each independent variable and a constant ϕ called the reference phase. The coefficients l , m , and ω of x , y , and t , respectively, bear the names of wave number in x , wave number in y , and frequency. They indicate how sharply the wave undulates in space and how fast it oscillates in time [10].

A wave crest is defined as the line in the (x, y) plane and at time t along which the signal is maximum ($a = +A$); similarly, a trough is a line along which the signal is minimum ($a = -A$). These lines and, in general, all lines along which the signal has a constant value at an instant in time are called phase lines. Figure depicts a few lines in the case of positive wave numbers l and m [10].

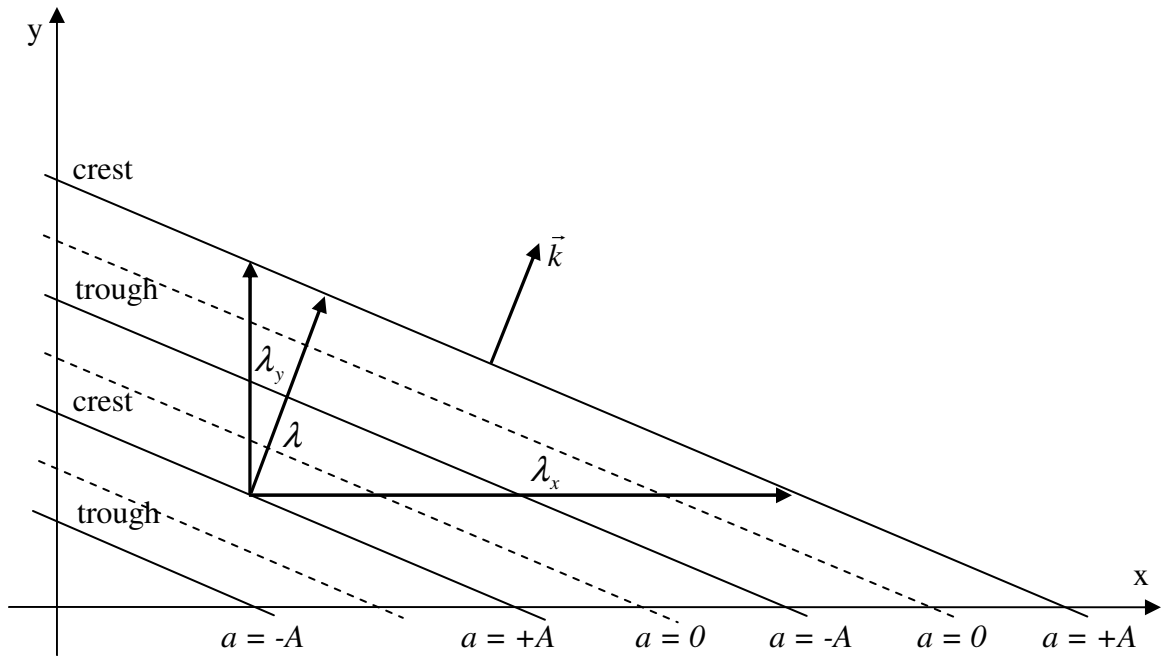


Figure 3.6 Phase lines of a two-dimensional wave signal at a given time

Because of the oscillatory behavior of the sinusoidal function, crest lines recur at constant intervals, thus giving the wavy aspect of the signal. The distance over which the signal repeats itself in the x -direction is the distance over which the phase portion lx increases by 2π , that is,

$$\lambda_x = \frac{2\pi}{l} \quad 3.24$$

Similarly, the distance over which the signal repeats itself in the y -direction is

$$\lambda_y = \frac{2\pi}{m} \quad 3.25$$

The quantities λ_x and λ_y are called the wavelength in the x - and y -directions. They are the wavelengths seen by an observer who would detect the signal only trough slits aligned with the x - and y -axes. The actual wavelength, λ , of the wave is the shortest

distance from the crest to nearest crest (Figure 3.6) [10]. Elementary geometric considerations provide

$$\frac{1}{\lambda^2} = \frac{1}{\lambda_x^2} + \frac{1}{\lambda_y^2} = \frac{l^2 + m^2}{4\pi^2} \quad \mathbf{3.26}$$

thus, the wavelength or the distance between waves is

$$\lambda = \frac{2\pi}{\sqrt{l^2 + m^2}} \quad \mathbf{3.27}$$

4 DATA SIMULATION

4.1 Scope

In this chapter we will perform image simulation before processing in order to understand its properties. Two types of images will be modeled: one-wave-train and three-wave-train. The Fourier Transform will be applied to the simulated image and the results will then be explained.

4.2 Simulation of the Waves

If we were to film the ocean's surface from above, the image we would obtain is the one we will process to extract the information we desire. Before developing an image processing algorithm, we need to study this type of image to see what visible signatures we may use to obtain valuable wave data.

4.2.1 One-wave-train simulation

To simulate an ideal type of image with only one-wave-train, we will apply the formula from Equation 3.22 which we discussed in an earlier section. However, instead of amplitude we will use the intensity of pixels in grayscale. The result is shown in Figure 4.1.

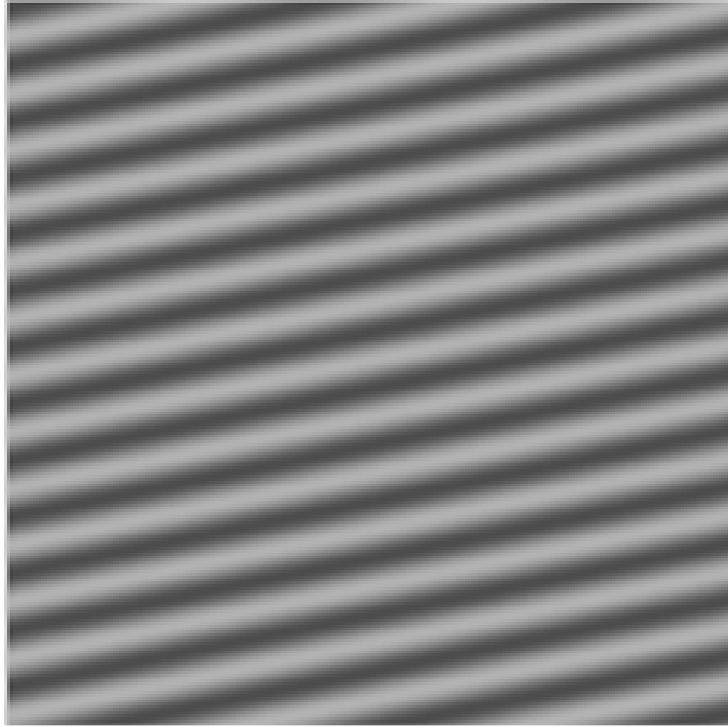


Figure 4.1 Ideal simulated image

In this image we have modeled the ideal situation: three horizontal wavenumbers and thirteen vertical wavenumbers are projected on the image plane. Looking at the image in Figure 4.1, one can tell at a glance what kind of visible information it is possible to obtain since one can easily count horizontal and vertical wavenumbers. Applying the formula from Equation 3.27 gives us the wavelength (distance between waves). Knowing wavenumbers, we can also find the wave direction (Equation 4.1).

$$\alpha = \arctan\left(\frac{m}{l}\right) \quad 4.1$$

where l and m , as stated before, are horizontal and vertical wavenumbers respectively.

Since the image has spatially periodic properties, we propose to process it in the wavenumber domain because it is easier to estimate the direction and wavelength of the waves by looking at the wavenumber pairs associated with the highest amplitudes (intensities), as shown in Figure 4.2 and Figure 4.3, where 2-D FFT was applied on the simulated original image from Figure 4.1 and the absolute values were taken to obtain the power spectrum of the image.

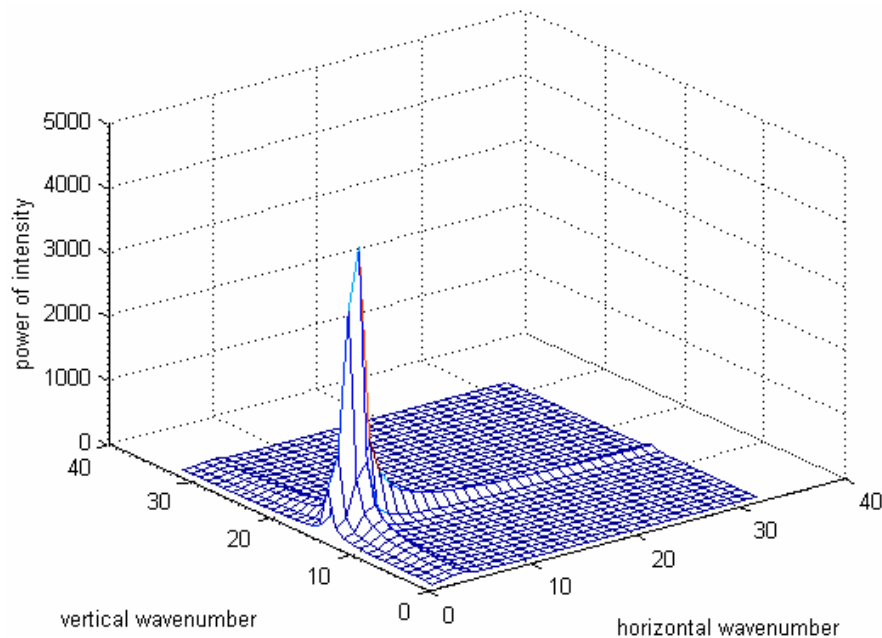


Figure 4.2 Power spectrum of the simulated image in 3-D

As one can see, the X - and Y -coordinates of the peak (highest intensity in grayscale) of the power spectrum exactly corresponds to the numbers of waves in horizontal and vertical directions respectively.

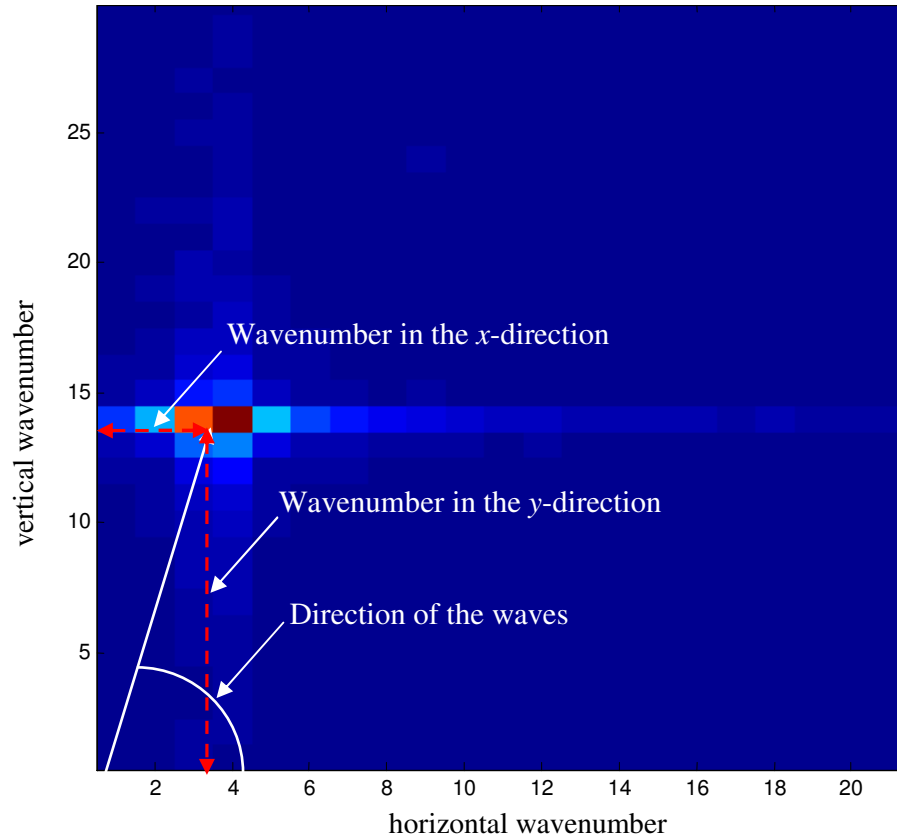


Figure 4.3 Power spectrum of the simulated image in 2-D

4.2.2 *Three-wave-train simulation*

In the previous section, we modeled the simplest ideal situation, where we simulated one train of ocean surface waves. This form is seen very rarely when it comes to real ocean dynamics. The ocean is a more complicated system where multiple physical processes are taking place. Looking out to sea from the shore on the surface of the ocean we easily notice how sea surface texture varies under different weather conditions. Usually, the ocean surface in nearshore waters is represented by several different wave trains. One type might originate from storms quite far away (perhaps thousands of

kilometers offshore); others might derive from local conditions, such as those formed by winds, and so forth. However, oceanographers and meteorologists are ordinarily interested in obtaining information from no more than the three most defined wave trains. Thus, by adding two more wave trains to the original image from Figure 4.1, we may derive the image shown in Figure. 4.4.

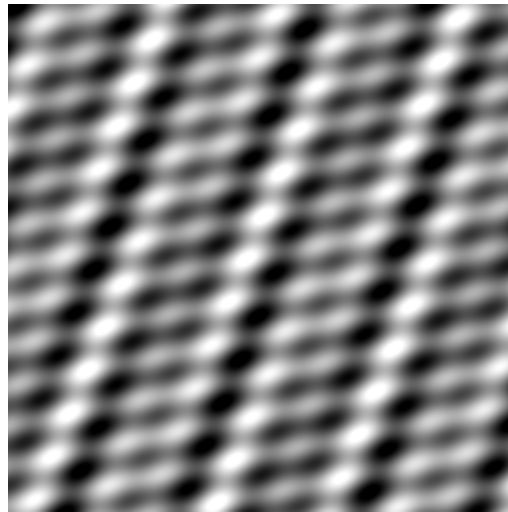


Figure 4.4 Three-wave-train simulated image

Visually it is quite difficult to distinguish the number of wave trains and their properties, such as wave period and wave direction. Application of 2-D FFT will help to solve this problem. Results of this application are shown in Figures 4.5 and 4.6.

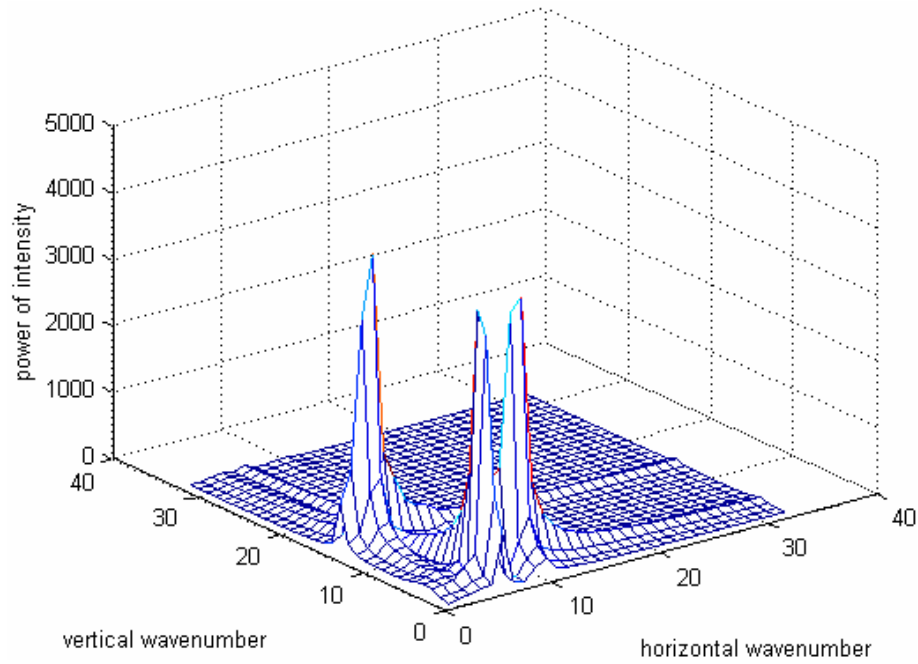


Figure 4.5 Power spectrum of the three-wave-train simulated image in 3-D

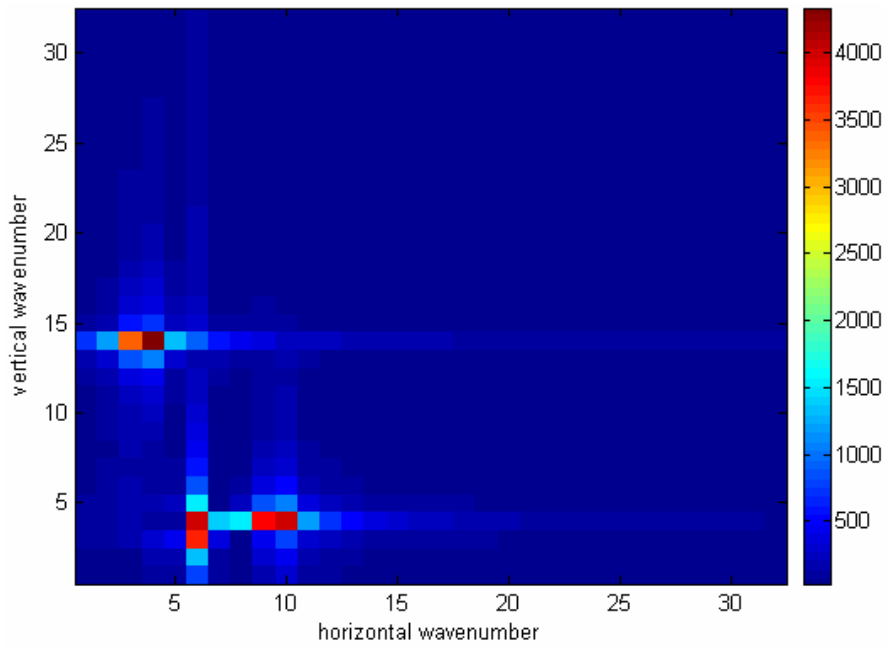


Figure 4.6 Power spectrum of the three-wave-train simulated image in 2-D

As mentioned previously, the coordinates of the peaks in Figures 4.5 and 4.6 correspond to wavenumbers of different wave trains. To conclude from the above paragraphs, the first step before developing an algorithm was to model the image we might have looking to sea surface waves from top. This gave us some conceptual ideas, what is the best way to process it to obtain the wave parameters.

5 REAL IMAGE ACQUISITION

5.1 Scope

This chapter will discuss the stages involved in retrieving the nearshore sea surface wave image from a video camera and its transfer to a server. For the purposes of this work the phrase “observation system” will refer to the combined video camera and network router, a device that will be described later in the chapter. The steps discussed will include requirements for a location to install an observation system, the installation itself, and testing results.

5.2 Description of an Observation System

5.2.1 Observation system diagram

To obtain a useful image of the nearshore zone, a video camera has to be mounted in the manner shown in Figures 5.1 and 5.2

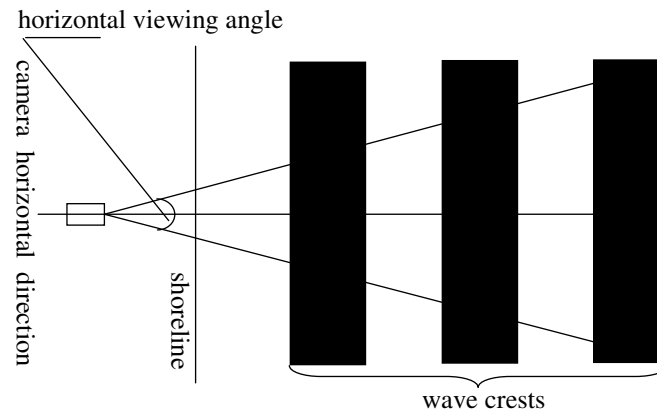


Figure 5.1 Schematic top view of the system

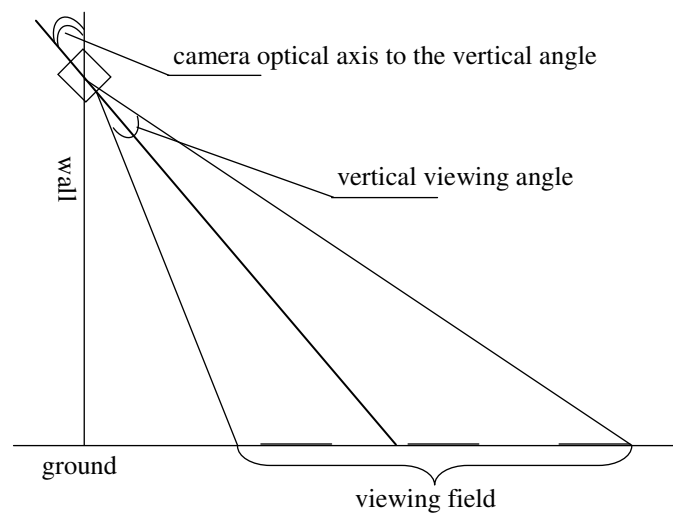


Figure 5.2 Schematic side view of the system

5.2.2 Observation system components

In order to make image processing possible, one first needs to receive the images of the sea surface waves and then devise a way to transfer them to the server that will process them. The primary solution is to have remote access to a video camera over the Internet. Thus the observation system needs a digital video camera, called an IP camera,

that has the ability to capture still images while connected to a network. Further, a network router is needed to provide remote access to the camera from the outside. The following diagram in Figure 5.1 shows the connected system components.

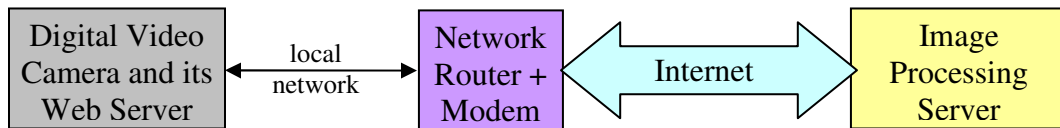


Figure 5.3 Connected components of the observation system

Before purchasing the necessary equipment, the following criteria were established:

- a component had to satisfy our project’s needs;
- it had to be relatively inexpensive; and
- it had to be reliable.

After some market research, the items in Table 5.1 were selected.

TABLE 5.1 Equipment list

Item Picture	Item ID	Total Price
	Toshiba IK-WB11A Indoor/Outdoor Wireless Network Camera	~ \$570
	Linksys Wireless-G Broadband Router - WRT54G	~ \$80

The Appendix lists the most important specifications of both the Toshiba IK-WB11A digital video camera and the Linksys WRT54G Wireless Router.

As the specifications point out, the video camera and the network router have two modes to connect, one by means of a twisted pair network cable (RJ-45) and the other by way of the wireless 802.11b standard. These options make the installation more flexible; if the modem is located quite far away from the video camera, one can still connect to the camera via wireless network. Of course, in most situations a wired connection is preferable because of its greater reliability.

Obviously, to make the observation system function correctly, the equipment has to be set up properly. First of all, the network router, connected to an ISP cable modem, must have a static Internet IP address accessible from the outside. The ISP is responsible for this connection. The router and the camera form the local network, with IP addresses visible only within this local network. As implied above, the router will have two IP addresses, one local, visible only for the video camera, the other a global IP address, visible to any computer connected to Internet. The video camera should have its own Web and FTP servers to provide easier access via HTTP or FTP protocols respectively. This means that if one knows the IP address of the camera, one can obtain the images using any Internet browser or FTP-client application installed on a PC. Several types of connection are possible:

- the PC is connected directly to the camera;

- the PC and the camera are within the same local network;
- the PC and the camera are in the different subnetworks. This setup requires the router to forward all incoming inquiries from another subnetwork (such as, in our case, the Internet itself) to the video camera as if they were generated by the router within the same local network.

Since the present research project required our image processing PC to be located remotely, our network router was configured as defined by the third type of connection.

5.2.3 Location requirements

This thesis proposes an approach that, like any other system, has some specific requirements and restrictions for its installation and maintenance. For example, the location of the observation system mounting has the following requirements:

- the site should be secure enough for permanent system installation;
- it must have facilities for connecting to the Internet;
- the waves to be recorded at the site have not yet been affected by reefs or other obstacles.

With these requirements in mind, a most interesting location for observing waves in Puerto Rico would be on the northern part of the island, almost anywhere along that shoreline. One such location—an apartment 30 meters inland and facing the ocean at 15-meters' height—was found in Isabela. Permission to use the site was facilitated by the

fact that the apartment was owned by a friend, Rita Peralta. The picture in Figure 5.4 shows the site where the observation system was installed.



Figure 5.4 Location of the observation system

Although the apartment was already Internet connected by means of a cable modem, the quality of service provided by the ISP needed improvement. Nevertheless, it was good enough to implement and test the system.

An aerial picture of the site, taken in 1999, is shown in Figure 5.5.



Figure 5.5 Aerial view of the site

Although this photo does not accurately represent a contemporary view of the site, the bathymetry of the area completely satisfies the requirements for the location of an observation system (Figure 5.6).

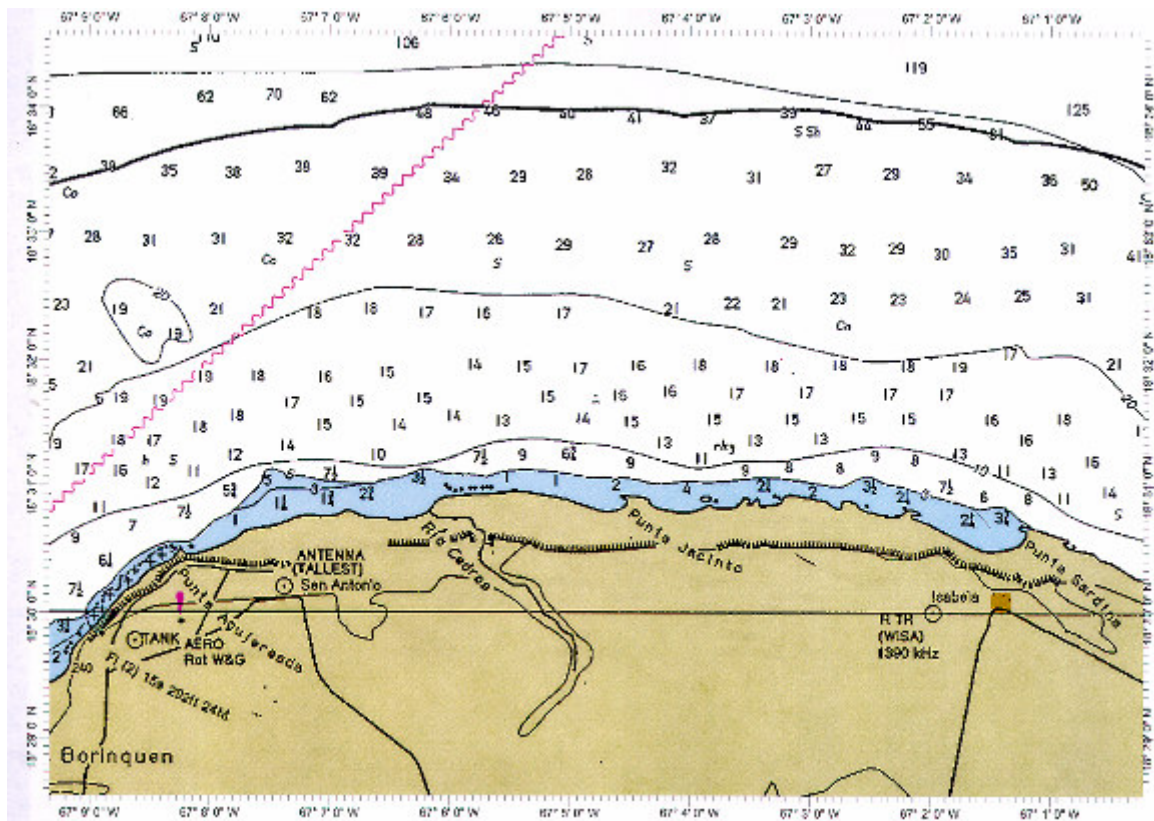


Figure 5.6 Isabela bathymetry chart

5.2.4 System mounting

After defining the type of equipment needed and the location requirements for the system mounting, the next stage is the installation process which consists of the following steps:

- mounting the video camera to the wall of the balcony facing the ocean;
- drilling holes in the wall to wire it up to the router;
- configuring the equipment;
- testing the connection.

Images in Figure 5.7 and Figure 5.8 show the video camera mounted to the wall.



Figure 5.7 Front view of the mounted camera

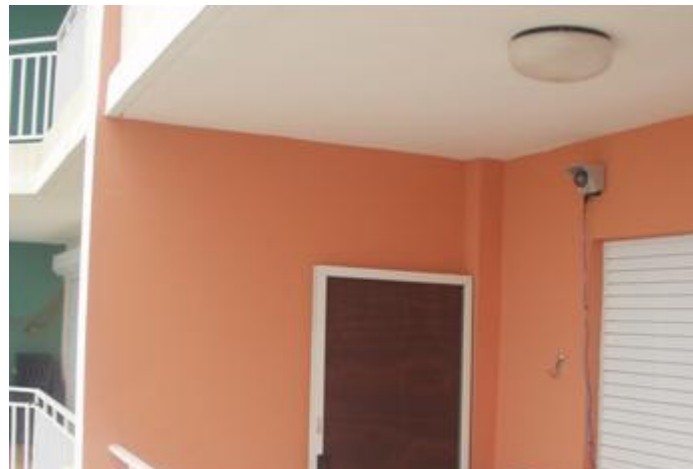


Figure 5.8 Side view of the camera

The configuration of the video camera and the router includes the following stages:

- using the camera settings to reduce image resolution from 1280 x 960 pixels to 640 x 480 pixels in order to retrieve a complete image. This reduction was necessitated by the presence of a poor Internet connection;
- assigning a local static IP address to the camera using the router's setting;

- assuring that the ISP had assigned a static Internet IP address for the router;
- enabling and configuring the forwarding function on the router;

After completion of the configuration, the system was successfully tested by retrieving images on the remote PC. Figure 5.9 shows an image with a resolution of 640 x 480 pixels recorded by the video camera.



Figure 5.9 Image from the video camera

6 REAL IMAGE PROCESSING

6.1 Scope

This chapter contains a detailed description of the general approach for extracting wave parameters, such as wave period, wave height, and wave direction, out of still images from the video camera. Some results are presented later in this chapter.

6.2 Algorithm description

6.2.1 Image preprocessing

The typical original image obtained from our observation system is shown in Figure 5.8 in the previous chapter. Before applying a 2-D FFT, the image needs to be cropped and transformed from a perspective to an orthogonal projection. The diagram in Figure 6.1 shows a sequence of the general stages needed to prepare the image for 2-D FFT transformation.

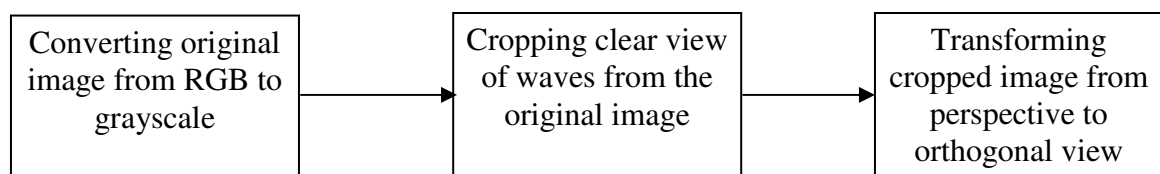


Figure 6.1 Image preprocessing stages

Converting the original image from RGB to grayscale is necessary because it is easier to work with intensities in one scale, when we are not interested in colors. Cropping the image is very important, because the vertical and horizontal viewing angles of the camera

are too wide and some unnecessary visual information like skies, ceiling, wall, and trees on the beach may be interpreted by the perspective transformation algorithm in an undesirable way. An example of a cropped grayscale image is shown in Figure 6.2.

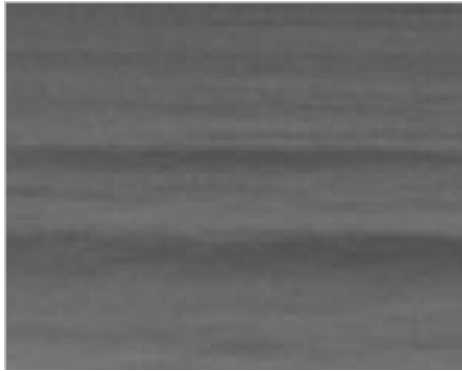


Figure 6.2 Cropped gray-scale image

After the clear view of the nearshore waves has been cropped from the original image, a perspective to orthogonal projection transformation has to be applied. In order to make this transformation, we need to know the following parameters of the video camera:

- focus length;
- diagonal of the camera's CCD matrix;
- resolution ratio of the camera (horizontal number of pixels to vertical);
- viewing angle of the camera;
- vertical angle of the camera to the surface (tilt);

Some of these given values can be obtained from the specifications given in Table 5.2, where, for example, the focal length is stated as $f = 6 \text{ mm}$, the diagonal of the CCD matrix is 0.5 inches (1.27 mm), and the resolution ratio is $4/3$ (640 to 480). In addition to

these values, the vertical viewing angle of the video camera can be found from Equation 6.1, where y is a vertical dimension of the CCD matrix.

$$\beta = 2 \arctan\left(\frac{y}{2f}\right) \quad \mathbf{6.1}$$

The tilting angle of the camera may be determined by Equation 6.4, covered later in this chapter. With this information gathered, a general perspective to orthogonal projection transformation, as described earlier (Equation 3.20), can be applied. It is assumed that the horizontal angle of the video camera to the sea shore is 90° . The result of this transformation as applied to the cropped image (Figure 6.2) is shown in Figure 6.3.



Figure 6.3 Orthogonal view image

6.2.2 Obtaining wave period and wave direction

To obtain parameters of the wave, such as wave period (distance between waves) and wave direction, the stages illustrated in Figure 6.4 have to be performed.

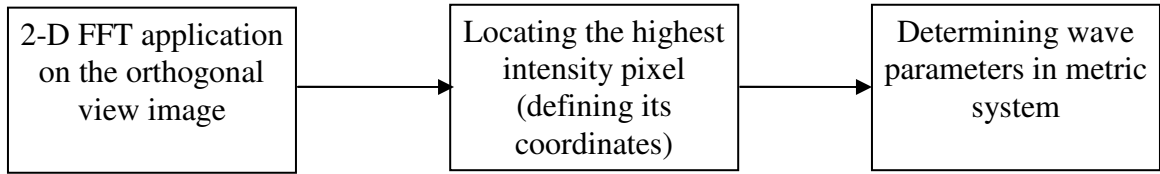


Figure 6.4 Image processing final stages

Results of applying 2-D FFT on the image (Figure 6.3) are illustrated in Figures 6.5 and 6.6.

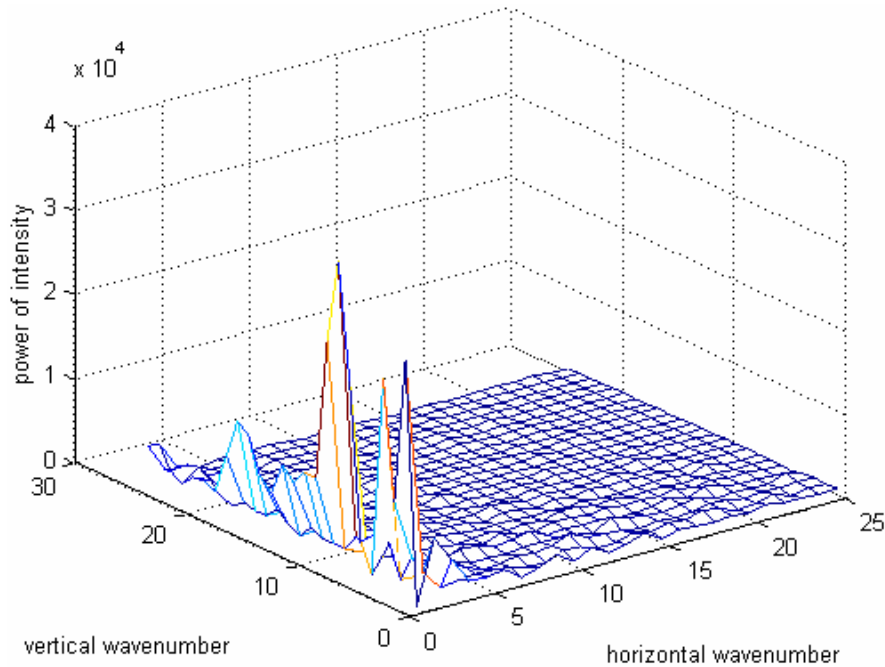


Figure 6.5 Power spectrum of the image in 3-D

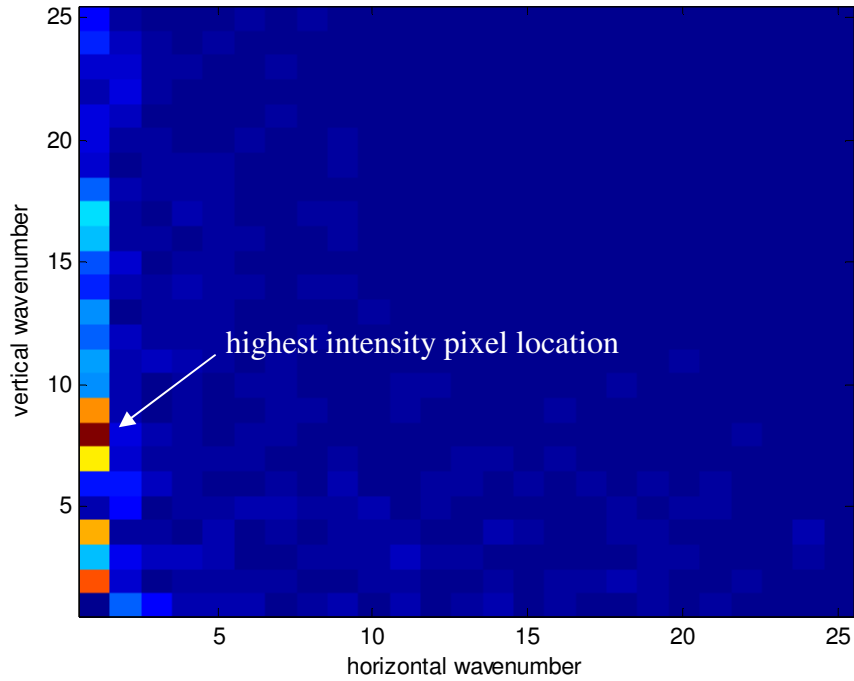


Figure 6.6 Power spectrum of the image in 2-D

We consider wave crests to be pixels with the highest intensity in grayscale. Horizontal and a vertical wavenumbers can be easily found by picking the coordinates of a pixel of highest power (intensity) from the wavenumber domain matrix (Figure 6.5). It is easily seen, that the vertical wavenumber is 8 and the horizontal is 0. The last step is to calculate a period and a direction for the waves. The direction can be calculated using a simple formula, given in Equation 4.1. In this particular case it will be 90° to the shore. The wavelength can be obtained from a formula, given in Equation 3.27, substituting with a vertical viewing dimension d , in other words the real distance in meters of the cropped viewing field in the vertical dimension (Equation 6.2).

$$\lambda = \frac{d}{\sqrt{l^2 + m^2}} \quad 6.2$$

To convert the image dimensions to real-world physical dimensions in meters, a GPS device may be used to measure the coordinates (latitude and longitude) of at least one selected point in the camera's viewing field, the coordinates of the camera and its height. To perform this, two people were used. One took the role of an object in the viewing field of the camera, measuring the coordinates of himself with the GPS (Figure 6.7). The other one was storing images on the computer and the coordinates of the "object". "Walkie-talkie" radios were used for communication. Now, when the coordinates of the camera and the object are known, the shortest distance between them (d), called the great-circle distance, can be found from Equation 6.3 [13], where δ_1 and δ_2 are latitudes and longitudes of these two points, and r is an average great-circle radius of curvature, a constant value which equals 6372.795 km.

$$d(\delta_1, \varphi_1, \delta_2, \varphi_2) = r \arccos(\sin \delta_1 \sin \delta_2 + \cos \delta_1 \cos \delta_2 \cos(\varphi_1 - \varphi_2)) \quad \mathbf{6.3}$$

Now we have all the necessary values to find a tilting angle of the camera which can be obtained from the simple trigonometry Equation 6.4, where d is the distance between the camera (as if it were mounted on the ground) and the nearest point on the viewing plane, h is the height of the camera and ψ is the camera's viewing angle.

$$\psi = \arctan\left(\frac{d}{h}\right) + \frac{\beta}{2} \quad \mathbf{6.4}$$



Figure 6.7 Object location

The distance d from Equation 6.2 can now be easily found by replacing the variables from the general perspective transformation Equation 3.20 with the real values.

6.2.3 Obtaining relative wave height

To estimate the wave height we propose to use a pressure sensor deployed on the bottom of the nearshore waters within the viewing field of the video camera. The pressure sensor and the video camera will record the wave data at the same time during a half an hour period. A detailed description of the pressure sensor is given in the next chapter. We assume that the highest-valued power in the wavenumber spectrum (e.g., the red pixel in Figure 6.6) correspond to the highest amplitude waves in the corresponding video image. The concept is to estimate a transfer function (in our case a multiplicative

constant) between this power and the significant wave height as estimated from the pressure sensor data (see below for details).

To estimate this constant, all the images recorded by the video camera must be processed over the same time period that pressure is recorded. The interval between successive images is 30 seconds, so a total of 60 images were processed over the time period of 30 minutes. The result of this processing was a time series of power peaks shown in Figure 6.8.

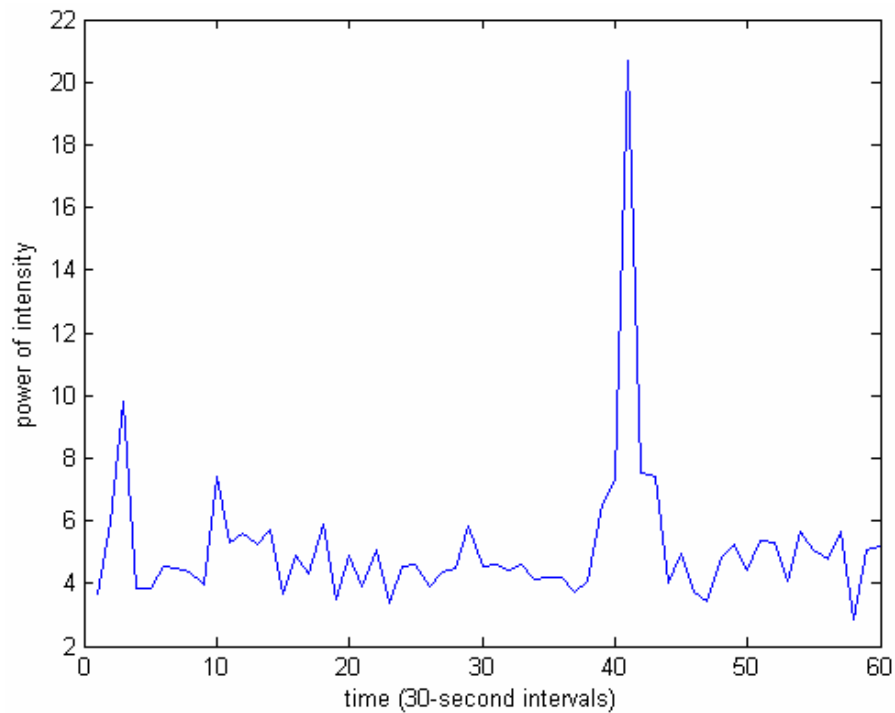


Figure 6.8 Time series of intensity power peaks

As one can see, the power values lie in the range 4 to 6 with an outlier, whose value is 21. The average of these power values (including the outlier) is ~ 5.14 . Now, the significant wave height recorded by the pressure sensor must be calculated. The

definition of significant wave height that is the average height of the highest 1/3 of the waves, denoted symbolically as $H_{1/3}$ [12].

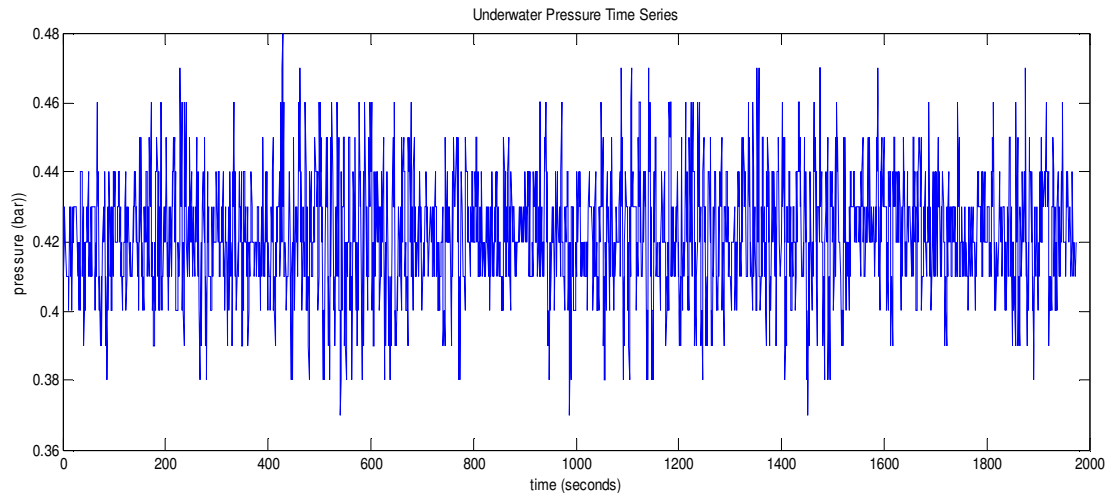


Figure 6.9 Pressure time series

The significant wave height from the data recorded by the pressure sensor shown in Figure 6.9 is ~ 0.6 m. Having the value of the average power and the value of the significant wave height, it is now possible to calculate the transfer function, K , between the significant wave height the average of the highest power values calculated from wavenumber power spectra. It is

$$K = 5.14/0.6 = \sim 8.57 \quad \mathbf{6.5}$$

Certainly, this technique is not extremely reliable; it depends on many factors that may affect the image and its intensity in different ways, such as the amount of sun light, or the angle and position of the sun. With reference to Puerto Rico, however, weather conditions throughout the year do not vary excessively, so we may consider this approach suitable for tropical and subtropical areas.

7 SYSTEM VALIDATION

7.1 Scope

This chapter contains a description of the validation method for the observation system, whereby a pressure sensor was deployed under the water in the viewing field of the camera and a pressure over time was measured.

7.2 Validation Method Description

7.2.1 Introduction

For validation of our observation system and the image processing algorithm described in the previous chapters, we propose to use a pressure sensor deployed on the bottom of the nearshore waters within the viewing field of the video camera. The pressure sensor and the video camera will record the wave data at the same time during a half an hour period.

7.2.2 Pressure sensor overview

The pressure sensor we use in our research is the DST milli - TD logger by Star-Oddi Marine Device Manufacturing. It is shown in Figure 7.1.

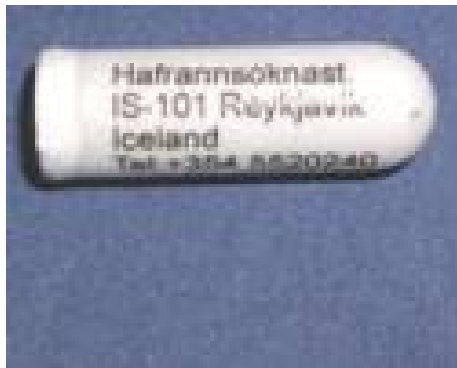


Figure 7.1 DST milli pressure sensor

The DST milli is a miniature data logger available with two sensors, temperature and depth (pressure). Data are stored into a non-volatile memory. All measurements are time related, utilizing a real time clock inside the DST.

Its basic features and specifications are:

- designed for temperature and depth measurements in the ocean and freshwater;
- ideal as a stand-alone logger for research in the ocean and lakes, or for temperature and pressure measurements in a liquid;
- weighs only 9.2 gm in air and 5 gm in water;
- dimensions are 38.4 mm (length) x 12.5 mm (diameter);
- memory capacity is 21,738 measurements per sensor;
- sampling interval ranges from 1 second to 90 hours;
- temperature range is from -1°C to +40°C (30°F to 104°F). Outside ranges are available upon request;

- depth (calibration) range can be selected up to 900 m (2953 feet); and
- battery life of 3 years (typical).

7.2.3 Pressure sensor deployment

The pressure sensor was deployed at about 4 meters' depth in the field of view of the video camera. It was attached to the rock as illustrated in Figure 7.2.



Figure 7.2 Pressure sensor attached to a rock

7.2.4 Reading pressure data

The sensor was deployed for a period of 30 minutes recording the pressure. It was set to measure pressure with one second intervals. A total of 1975 measurements were taken. A special software package SeaStar for Windows, and a communication box were used to

configure the pressure sensor and to read the data out of it. The time series of the recorded data is shown in the previous chapter in Figure 6.9.

7.2.5 Pressure data analysis

The most valuable information for the present research taken from this set of data is a frequency distribution of different pressure values which will correspond to wave frequency. A Fast Fourier Transformation was applied to the pressure time series in order to obtain the power spectrum. The result is shown in Figure 7.5.

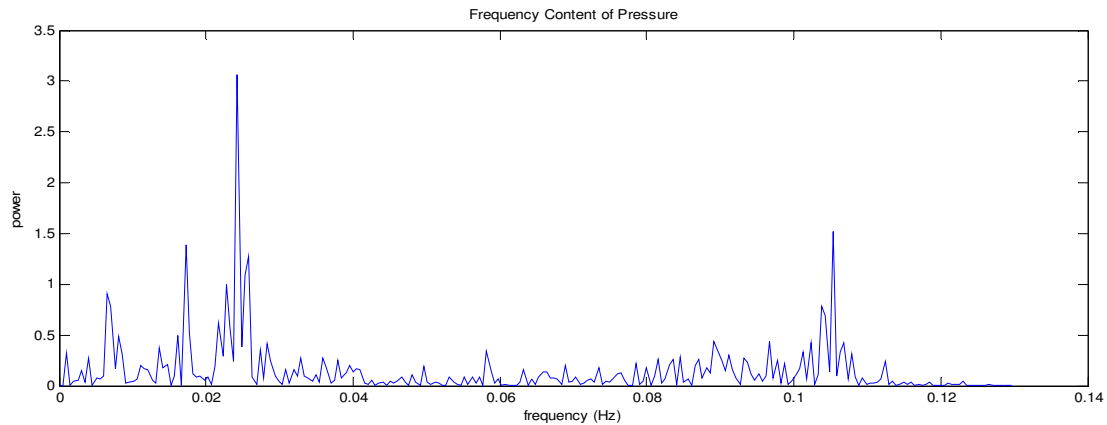


Figure 7.3 Power spectrum of the pressure time series

One can see, that there are two significant peaks. The second highest peak corresponds to waves with a frequency of just over 0.1 Hz. These are the ones that appear in the field of view of the camera (Figure 6.7). Knowing the depth of the water and the wave frequency, the wavelength can be calculated using the shallow-water dispersion relation given in Equation 7.1.

$$\lambda = \frac{\sqrt{gd}}{f} \quad 7.1$$

where d is the water depth, g is the acceleration due to gravity, f is the wave frequency, and λ is the wavelength [8]. Substituting these variables with the values $d = 4$, $g = 9.8$, and $f = 0.1$, we obtain a value for wavelength of ~ 63 meters.

7.2.6 System validation

When the wavelength is known, we are able to compare results obtained from the image processing algorithm. The calculated distance of the cropped view is ~ 530 meters and the wave number is 8 (Figure 6.6). Replacing the variables from Equation 6.2 with the obtained values we have (Equation 7.2):

$$\lambda = \frac{530}{\sqrt{8^2 + 0^2}} \approx 66 \quad 7.2$$

The wavelength obtained from the pressure sensor data in the previous paragraph is ~ 63 meters. The error is $\sim 5\%$.

8 CONCLUSIONS AND FUTURE WORK

This research project, involving the processing of images from a video camera pointed toward the nearshore surface of the ocean, presents an accurate and inexpensive solution for those investigators who might be interested in obtaining the wave parameters of nearshore surface waves, such as wave period and wave direction. The image processing algorithm proposed here is based on the 2-D Fast Fourier Transformation of images and finding wavenumbers in both horizontal and vertical direction. The method was validated by verifying the data obtained from the pressure sensor recording the wave frequency at the same time as the video camera.

Some restrictions apply to the method; most obviously, for example, the system is suitable only during the day-light and in relatively fair weather.

In future work an attempt will be made to extract information about relative wave-height, based on the length of wave foam breaking on beach. It may also be possible to detect tides from images that have been recorded by the video camera.

Bibliography

- [1] The UKCIP02 Scientific Report. Climate Change Scenarios for the United Kingdom, pages 13-14, April 2002.
- [2] D. Bush, R. Webb, L. Hyman, J. Gonzalez Liboy, and W. Neal. Living with the Puerto Rico Shore. Duke University Press, Durham and London, pages 26-27, 1995.
- [3] R.A. Holman. The application of video image processing to the study of nearshore processes. *Oceanography*, vol. 6 no. 3, pages 78-85, 1993
- [4] K.T. Holland, R.A.Holman, T. C. Lippmann, J. Stanley, N. Plant. Practical use of Video Imagery in Nearshore Oceanographic Field Studies. *IEEE Journal of Oceanic Engineering*, Vol. 22, No. 1, pages 81-92, January 1997.
- [5] R. C. Chandler. A wavelet based method for the extraction of sea wave orientation. *Oceans 2005*, proceeding no. 050214-10, 2005
- [6] J. Torres, J. Favela, F. J. Ocampo-Torres, A. Mascarenhas. Ocean Wave Parameter Retrieval from SAR Imagery Using Wavelet Analysis. *Geoscience and Remote Sensing Symposium Proceedings, 1998. IGARSS '98, 1998 IEEE International, Volume 2*, pages 965 – 967, 6-10 July 1998
- [7] R.C. Gonzalez, R.E. Woods. *Digital image processing. Second Edition*, Prentice-Hall, Inc. pages 1-2, 52-56, 2002
- [8] R. Fisher, S. Perkins, A. Walker and E. Wolfart. Hypermedia image processing reference. HIPR, <http://homepages.inf.ed.ac.uk/rbf/HIPR2/fourier.htm>, 2000.
- [9] W. K. Pratt. *Digital image processing. Third Edition*, John Wiley and Sons, Inc. pages 386-392, 2000
- [10] Benoit Cushman-Roisin. *Introduction to geophysical fluid dynamics. First Edition*, Prentice-Hall, pages 280-284, 1994
- [11] R.H. Stewart. *Introduction to physical oceanography. Department of Texas A&M University*, pages 283-285, 2000.
- [12] Wikipedia, the free encyclopedia. http://en.wikipedia.org/wiki/Great-circle_distance , March 2005.

[13] T. Watkins. Spherical Geometry and Trigonometry. <http://www.applet-magic.com/sphere.htm>

Appendix

This appendix includes:

1. Toshiba IK-WB11A specifications.
2. Linksys WRT54G Wireless Router specifications.
3. Derivation of great-circle distance formula 6.3.
4. Program for one-wave train image simulation.
5. Program for three-wave-train image simulation.
6. Program that processes real images.
7. Program that reads the data from the pressure sensor and calculates the significant wave height.

Toshiba IK-WB11A specifications

IMAGING

Image Sensor.....	1/2" CCD
Pixel Count	1.45 Megapixel
Focal Length	f=6.0mm
F-Stop	F=1.4
Focusing Range	31.5" to infinity
Minimal Illumination	1 Lux (Normal), 0.03 Lux (w/slow shutter)
Compression	JPEG (3 mode)
AGC	Yes
Backlight Comp.	Yes

Image Sizes

SXVGA:	1280x960
XGA:	800x600
VGA:	640x480
QVGA:	320x240
QQVGA:	160x120

CONTROLS

Pan	112° (+56 to -56)
Tilt	54° (+5 to -49)
Digital Zoom	5x
Preset Position	10 Positions

Maximum Frame Rates

1280x960	7.5 fps maximum
800x600	7.5 fps maximum
640x480	7.5 fps maximum
320x240	30 fps maximum
160x120	30 fps maximum
Auto B/W	Yes (selectable)
Motion Alarm	Yes
Normal Record	Yes
E-Mail Notification	Yes
Shutter Speeds.....	AES, Selectable, 1/120, 1/60, 1/30, 1/20, 1/15, 1/8, 1/4, 1/2, 1, 2, 4 seconds
Working Temperature	-4° to 122° F
Humidity	90% or less
Weather Resistant Rating	IPX3

CONNECTIVITY

Ethernet	RJ45 (10Base-T/100BASE-TX)
Wireless	IEEE802.11b
Protocols	TCP/IP, HTTP, SMTP, DNS, DHCP, NTP, ARP, ICMP, syslog, UDP/IP, FTP

Linksys WRT54G Wireless Router specifications

Standards.....	IEEE 802.3, IEEE 802.3u, IEEE 802.11g, IEEE 802.11b
Channels	11 Channels (US, Canada), 13 Channels (Europe), 14 Channels (Japan)
Ports/Buttons	Internet: One 10/100 RJ-45 Port, LAN: Four 10/100 RJ-45 Switched Ports, One Power Port, One Reset Button
Security Features	Stateful Packet Inspection (SPI), Firewall, Internet Policy
Wireless Security	Wi-Fi Protected Access™ (WPA), WEP, Wireless MAC Filtering

Derivation of great-circle distance formula

The problem is to determine the great circle distance between two points given their latitudes and longitudes [14]. Let φ_1 and φ_2 be the latitudes of the two points and θ_1 and θ_2 their longitudes. The basis for the determination of the angular separation of the two points on the great circle which connects them is the Law of Cosines for plane triangles.

The Law of Cosines for any triangle states

$$a^2 = b^2 + c^2 - 2bc \cos(A)$$

When the points are on a great circle this formula reduces to:

$$a^2 = 2r^2(1 - \cos(A))$$

or

$$\cos(A) = (1 - (a/r)^2)/2$$

Therefore if we can find the straight line (Euclidean distance between the two points) we can find their great circle angular separation A. The Euclidean distance between the two points can be found from their Euclidean coordinates, (x_1, y_1, z_1) and (x_2, y_2, z_2) , by the formula

$$a^2 = (x_2 - x_1)^2 + (y_2 - y_1)^2 + (z_2 - z_1)^2$$

The Euclidian coordinates are given by the transformation

$$x = \cos(\theta)(r \cos(\varphi))$$

$$y = \sin(\theta)(r \cos(\varphi))$$

$$z = r \sin(\varphi)$$

Thus

$$(a/r)^2 = (\cos(\theta_2)\cos(\varphi_2) - \cos(\theta_1)\cos(\varphi_1))^2 + (\sin(\theta_2)\cos(\varphi_2) - \sin(\theta_1)\cos(\varphi_1))^2 + (\sin(\varphi_2) - \sin(\varphi_1))^2$$

When the squared terms in the above expression are expanded we obtain from the first term, in addition to the cross product term, terms of the form

$$\cos^2(\theta_i)\cos^2(\varphi_i)$$

for $i= 1$ and 2 .

These combine with terms from the second squared term of the form

$$\sin^2(\theta_i)\cos^2(\varphi_i)$$

to give terms of the form,

$$\cos^2(\varphi_i).$$

These, in turn, combine with the terms from the third squared term to give $(1+1)$. Thus,

$$(a/r)^2 = 2 - 2\cos(\theta_2)\cos(\theta_1)\cos(\varphi_2)\cos(\varphi_1) - 2\cos(\varphi_2)\cos(\varphi_1) - 2\sin(\varphi_2)\sin(\varphi_1)$$

Thus the formula for the cosine of the great circle angular separation reduces to:

$$\cos(A) = \cos(\theta_2)\cos(\theta_1)\cos(\varphi_2)\cos(\varphi_1) + \sin(\theta_2)\sin(\theta_1)\cos(\varphi_2)\cos(\varphi_1) + \sin(\varphi_2)\sin(\varphi_1)$$

With rearrangement this can be written as:

$$\cos(A) = [\cos(\theta_2)\cos(\theta_1) + \sin(\theta_2)\sin(\theta_1)]\cos(\varphi_2)\cos(\varphi_1) + \sin(\varphi_2)\sin(\varphi_1)$$

The term within the brackets can also be expressed in terms of the difference of longitudes. Hence the standard formula for great circle angular separation:

$$\cos(A) = \sin(\varphi_2)\sin(\varphi_1) + \cos(\varphi_2)\cos(\varphi_1)\cos(\theta_2 - \theta_1)$$

Program for one-wave-train image simulation

```
clear all;
N = 256;
y1=0;
Lx=100; % horizontal wave period
Ly=20; % vertical wave period
Lx2=30; % horizontal wave period (2-d wave train)
Ly2=80; % vertical wave period
Lx3=50; % horizontal wave period (3-d wave train)
Ly3=100; % vertical wave period

Kx = 2*pi/Lx;
Ky = 2*pi/Ly;
Kx2 = 2*pi/Lx2;
Ky2 = 2*pi/Ly2;
Kx3 = 2*pi/Lx3;
Ky3 = 2*pi/Ly3;

for k=1:10
    for x = 1:N
        for y = 1:N
            I = 0.5 + 0.2*(sin(Kx*x + Ky*y + k)); % + sin(Kx2*x + Ky2*y + k) + sin(Kx3*x +
            Ky3*y + k));
            fake_image(y,x) = I;
        end
    end
    im_arr{k}=fake_image; % adding an image matrix to a cell array
    im_arr_fft{k} = fft2(im_arr{k}); % performing 2D FFT and creating a cell array of ABS
    FFTs
    first(k) = im_arr_fft{k}(1,1);
    im_arr_fft{k}(1,1) = 0;
end

fft_sum=0;

% averaging the FFTs

for k=1:10
    fft_sum = fft_sum + im_arr_fft{k};
end

fft_avr = (fft_sum/10);
```

```

%im_arr_fft{1}(1:256, 20:256) = 0;

%im_arr_fft{1}(20:256, 1:256) = 0;

xx = 1:N/6;
%figure;
%imshow(im_arr{1});
[u v] = meshgrid(xx,xx);
%[u1 v1] = meshgrid(256,256);
figure(1);
imagesc(abs(im_arr_fft{1}(1:N/6, 1:N/6)));
figure(2);mesh(u,v, abs(im_arr_fft{1}(1:N/6, 1:N/6)));
figure(3); imshow(fake_image);
% mesh(u1,v1, im_arr{1});
%im_rev = abs(iff2(fft_avr));
%figure;
%imshow(im_rev);

```

Program for three-wave-train image simulation

```
clear all;
N = 256;
y1=0;
Lx=100; % horizontal wave period
Ly=20; % vertical wave period
Lx2=30; % horizontal wave period (2-d wave train)
Ly2=80; % vertical wave period
Lx3=50; % horizontal wave period (3-d wave train)
Ly3=100; % vertical wave period

Kx = 2*pi/Lx;
Ky = 2*pi/Ly;
Kx2 = 2*pi/Lx2;
Ky2 = 2*pi/Ly2;
Kx3 = 2*pi/Lx3;
Ky3 = 2*pi/Ly3;

for k=1:10
    for x = 1:N
        for y = 1:N
            I = 0.5 + 0.2*(sin(Kx*x + Ky*y + k) + sin(Kx2*x + Ky2*y + k) + sin(Kx3*x + Ky3*y
+ k));
            fake_image(y,x) = I;
        end
    end
    im_arr{k}=fake_image; % adding an image matrix to a cell array

    im_arr_fft{k} = fft2(im_arr{k}); % performing 2D FFT and creating a cell array of ABS
    FFTs
    first(k) = im_arr_fft{k}(1,1);
    im_arr_fft{k}(1,1) = 0;
end

fft_sum=0;

% averaging the FFTs

for k=1:10
    fft_sum = fft_sum + im_arr_fft{k};
end
```

```
fft_avr = (fft_sum/10);
```

```
xx = 1:N/4;
```

```
%figure;
```

```
[u v] = meshgrid(xx,xx);
```

```
figure(1); imagesc(abs(im_arr_fft{1})(1:N/4, 1:N/4)); % displaying the result in 2-D
```

```
figure(2); mesh(u,v, abs(im_arr_fft{1})(1:N/4, 1:N/4)); displaying the result in 3-D
```

```
figure(3); imshow(fake_image);
```

Program that process real images

```
clear all;

file_name=strcat('video/im1000055.jpg');
origin = rgb2gray(imread(file_name));

xmin = 230;
ymin = 120;
width = 150;
height = 120;

gray = imcrop(flipud(origin), [xmin, ymin, width, height]);
dim = size(gray); %getting dimensions of the image to "dim" vector
% setting the dimensions of the CCD matrix of the video network camera Toshiba IK-
WB11A
focal = 6; % focal length in mm
b = 7.62; % vertical length of the camera's viewplane in mm;
pixn = dim(1);
d = sqrt(focal*focal+(b/2)*(b/2)); % distance from the light source to the vertical edge of
the camera's viewplane in mm;
alpha = 2*atan(b/(2*focal)); %vertical viewing angle of the camera;
beta = pi/4;
b1 = b*(sin(pi/2+alpha/2)/sin(pi/2-alpha/2-beta));
coeff = b/pixn; % the number of mm in one pixel;
coeff_new = b1/pixn; % the number of mm in one pixel in projected plane;

% cropped = imcrop(gray, [xmin ymin width height]);

for x = 1:dim(2)
for y2 = 1:dim(1)
y = y2*coeff_new; % calculating the distance in mm to the point on the projected plane;
d1 = sqrt(y*y+d*d-2*y*d*cos(pi/2-alpha/2+beta));
gamma = asin(d*sin(pi/2-alpha/2+beta)/d1);
y1 = y*sin(gamma)/sin(pi-gamma-beta);
y1_coord = floor(y1/coeff);
delta = y1/coeff-y1_coord;
if (y1_coord==dim(1))
ip_inten = gray(y1_coord,x);
else
ip_inten = gray(y1_coord,x) - (gray(y1_coord,x)-gray(y1_coord+1,x))*delta; %
calculating intensity of the interpolation pixel
end
```

```

newim(y2,x)=ip_inten;
%newim(y2-ymin+1,x-xmin+1)=gray(y2,x);
end
end

fft_crop = abs(fft2(flipud(newim)));

first = fft_crop(1,1);

fft_crop(1,1) = 0;

xx = 1:25;
yy = 1:25;

% final = 100*abs(iff2(fft_crop));

[u v] = meshgrid(xx,yy);

figure; mesh(u,v, abs(fft_crop(1:25, 1:25)));
%figure; imshow(flipud(newim));
figure; imagesc(fft_crop (1:25, 1:25));
%figure; imshow(flipud(gray));

```

Program that reads the data from the pressure sensor and calculates the significant wave height

```
clear all;
i = 1;
i_cr = 1;
crests_sum = 0;
data = fopen('underw.txt', 'rt');
while feof(data) == 0
    a{i} = fgetl(data);
    data_arr(i)=str2num(a{i}(31:32)); % reading data from the file recorded by the pressure
sensor
    i=i+1;
end
fclose(data);

data_arr = data_arr/100;

for ind=1:(i-1)
    if (data_arr(ind)>0.42)
        crests(i_cr)=20*(data_arr(ind)-0.42); % creating a new array of all wave crest heights;
        i_cr=i_cr+1;
    end
end

crests_sort=sort(crests, 'descend'); %sorting the elements of the wave heights in
descending order

one_third=floor(i_cr/3); %calculating the value of 1/3 of the wave crests;

for i_s = 1:one_third
    crests_sum = crests_sum + crests_sort(i_s); %calculating the sum of the 1/3 highest
wave crests
end

swave_h = crests_sum/one_third; %calculating the significant wave height;

figure (1);
plot(data_arr);
title('Underwater Pressure Time Series')
xlabel('time (seconds)')
ylabel('pressure (bar))')
```

```
Y = fft(data_arr,512);  
Pyy = Y.* conj(Y);  
Pyy(1)=0;  
f = 0:256;  
figure;  
plot(f/i,Pyy(1:257));  
title('Frequency Content of Pressure')  
xlabel('frequency (Hz)')  
ylabel('power')
```